Controlled-error approximations for surface diffusion of interacting particles with applications to pattern formation

Yannis Pantazis and Markos Katsoulakis

CONTROLLED-ERROR APPROXIMATIONS FOR SURFACE DIFFUSION OF INTERACTING PARTICLES WITH APPLICATIONS TO PATTERN FORMATION

YANNIS PANTAZIS* AND MARKOS KATSOULAKIS†

Abstract. Microscopic processes on surfaces such as adsorption, desorption, diffusion and reaction of interacting particles can be simulated using kinetic Monte Carlo (kMC) algorithms. Even though kMC methods are accurate, they are computationally expensive for large-scale systems. Hence approximation algorithms are necessary for simulating experimentally observed properties and morphologies. One such approximation method stems from the coarse graining of the lattice which leads to coarse-grained Monte Carlo (GCMC) methods while Langevin approximations can further accelerate the simulations. Moreover, sacrificing fine scale (i.e. microscopic) accuracy, mesoscopic deterministic or stochastic partial differential equations (SPDEs) are efficiently applied for simulating surface processes. In this paper, we are interested in simulating surface diffusion for pattern formation applications which is achieved by suitably discretizing the mesoscopic SPDE in space. The proposed discretization schemes which are actually Langevin-type approximation models are strongly connected with the properties of the underlying interacting particle system. In this direction, the key feature of our schemes is that controlled-error estimates are provided at three distinct time-scales. Indeed, (a) weak error analysis of mesoscopic observables, (b) asymptotic equivalence of action functionals and (c) satisfaction of detailed balance condition, control the error at finite times, long times and infinite times, respectively. In this sense, the proposed algorithms provide a "bridge" between continuum (S)PDE models and molecular simulations Numerical simulations, which also take advantage of acceleration ideas from (S)PDE numerical solutions, validate the theoretical findings and provide insights to the experimentally observed pattern formation through self-assembly. Such phenomena are characterized by a complex energy landscape where the role of noise is critical in the emergent behavior of the system. The stochastic fluctuations of the proposed algorithms are directly derived from the microscopic model allowing us to explore all experimentally observed pattern morphologies starting from a uniform initial state.

Key words. Interacting particle systems, stochastic (partial) differential equations, Langevin approximation, surface diffusion, pattern formation.

1. Introduction.

Surface diffusion of interacting particles as well absorption, desorption, reaction, etc. can be accurately simulated using kinetic Monte Carlo (kMC) algorithms [1], [2]. In particular, Ising models are set on a lattice and each site of the lattice has an order parameter (spin) that describes the presence or not of a particle as well its type (Potts models) [3]. Surface diffusion is characterized by spin exchange between neighboring sites (Kawasaki dynamics) and depending on the rates of the process, kMC evolves the system towards the equilibrium states. However, microscopic simulation is computationally expensive when large spatiotemporal scales observed in real-life experiments are studied.

One approach of accelerating the microscopic simulation was developed in a series of papers [4], [5], [6] called coarse-grained Monte Carlo (CGMC) method. In CGMC setting, the microscopic lattice was coarse-grained and the spins was grouped into cells resulted in smaller number of system parameters. Rigorous error analysis was performed in [7] and [8] showing that the finite time error is controlled by the interplay of the coarsening factor, the temperature and the smoothness of the interaction potential. Particularly for surface diffusion, it was shown that coarse-graining resulted

*Mathematics and Statistics, University of Massachusetts, Amherst, MA, USA, pantazis@math.umass.edu.

†Math. and Stat., University of Massachusetts, Amherst, MA, USA and Dept. of Applied Mathematics, University of Crete, Greece and Institute of Applied and Comp. Math., FORTH, Greece, markos@math.umass.edu.

not only in the reduction of the number of system parameters but also in time acceleration (square of the coarsening factor faster). In general, CGMC works satisfactory for long range and mid range interaction lengths, however, it may produce erroneous results especially for short range interactions, nevertheless, recent variations of the basic CGMC algorithm have been proposed, trying to overcome this limitation [9]. Even though CGMC is a powerful tool for accelerating microscopic kMC algorithms, we are primarily interested in studying pattern formation on surfaces with the expected patterns having relatively small size. Thus, in order not to lose the necessary resolution of the patterns, we need to keep the coarsening factor small making CGMC method a rather inefficient approach.

Another approach to accelerate even further the microscopic simulations is to derive mesoscopic equations by letting the number of interacting particles tend to infinity. Mesoscopic equations for interacting particles are either deterministic or stochastic integro-differential equations. Deterministic PDEs have been used to study nucleation, pattern formation, alloys, etc. [10], [11], [12]. However, thermal fluctuations (i.e. noise) are important for studying the dynamics thus, more recently, stochastic PDEs (SPDEs) have been used [13], [14], [15], [16], [17]. For instance, Ostwald ripening was studied in [17] using an SPDE model. All kinds of numerical schemes such as finite differences, finite elements, finite volumes as well (pseudo-)spectral methods have been applied for the discretization of the studied (S)PDEs which leads to a system of ODEs in the deterministic case and to a system of SDEs in the stochastic case. Another technique to derive a system of SDEs that simulates microscopic processes is by a Langevin approximation of the master equation [18], [19]. Such a Langevin approximation was derived and studied for surface diffusion and Arrhenius dynamics in [20] where it was shown that not only the weak error but also the large deviation properties of the model are correctly handled. However, in the above studies few or no care was taken about the exact equilibrium (i.e. invariant) measure of the simulating process primarily because of the difficulty in satisfying detailed balance condition (DBC).

In this paper, we develop three different systems of SDEs which serve as approximation models of the microscopic surface diffusion process and additionally satisfy DBC. The first model is a second-order space-discretization of the mesoscopic SPDE which is also related with the coarse-grained Langevin (CGL) approximation of [20]. Even though it is a discretization scheme of the SPDE, we refer to this stochastic model as direct Langevin approximation model (DLM) because its local error is asymptotically of the same order as the CGL approximation. Furthermore, large deviation computations show that the action functional between DLM and the microscopic process are asymptotically equivalent thus, rare events and phase transitions are correctly represented [21]. However, DLM does not satisfy DBC hence its invariant measure so important for determining the equilibrium states or for applications such as sensitivity analysis of system parameters [22] is not known in general. Nevertheless, the structure of DLM allows the construction of a variant model which satisfy DBC. Indeed, the second system of SDEs named as perturbed Langevin approximation model 1 (PLM1) is derived by adding a "correction" term to the drift of DLM. Then DBC is satisfied and the invariant measure is easily obtained. However, the "correction" term depends on the coarsening factor hence the cost to be paid is that the local error is no more as accurate as the local DLM error which results in perturbed finite time dynamics.

The third model which is named PLM2 eliminates the effect of the "correction"

term by slightly perturbing the invariant measure in a controlled-error manner. For Metropolis dynamics, the "correction" term is of diffusion type thus the perturbation of the invariant measure is an additional higher order term to the entropy. The effect of this perturbation is that the interacting particle system is simulated at a slightly different temperature than the original! Similar but more complex perturbation of the invariant measure is also obtained for the Arrhenius dynamics. Overall, in any of the proposed models, the error performed either in finite times or in infinite times is controllable not only to the asymptotic limit but also for any coarsening factor and actually the interconnection between the finite and infinite time errors as highlighted by PLM1 and PLM2 models is one of the key findings of this paper.

Having derived the stochastic models, the final step in order to simulate and test them on computers is to discretize the time, too. Since our primal goal is to highlight the space-discretization properties, we keep the time-discretization as simple as possible. Thus a simple predictor-corrector (PC) Euler scheme which has 1st order weak convergence [23] is used. PC Euler which is a two step method can be thought as a compromise between an explicit and an implicit scheme. Higher order schemes such as Milstein's or derivative-free Runge-Kutta method could also be applied. However, higher order schemes are computationally expensive especially for high dimensional systems such as the studied.

The computational savings of the proposed models compared to the microscopic system come from many directions. Except for the computational acceleration due to the coarse-graining which as we already mention is rather limited due to the application we are interested in (i.e. pattern formation), there are two other important acceleration points. The first acceleration is that while in CGMC algorithms only one particle is allowed to hop between neighboring cells in a time step, in Langevin approximation more than one "particles" could change their positions on the lattice in a single time step. The second acceleration stems from the fact that in order to perform a time step the convolution between the interaction potential and the coarse-grained lattice configuration is needed to be computed. Convolution can be performed in Fourier space which results in huge computational savings especially when the interaction potential is long range. This feature is primarily an advantage of spectral methods which is integrated into our algorithms making eventually the computational cost independent of the interaction length.

Finally, the proposed Langevin approximation models are applied to the study of pattern formation phenomena. Such phenomena are characterized by a complex energy landscape [24], [25], [26] where the role of noise is critical in the emergent behavior of the system. The stochastic fluctuations of the proposed algorithms are directly derived from the microscopic model, they allow us to systematically explore all experimentally observed pattern morphologies through a self-assembly mechanism, starting from a uniform initial state (non-equilibrium dynamics). Indeed, using Morse-type interaction potential, which is an attractive/repulsive potential, at various parameter regimes, we were able to reproduce the experimentally observed 2D images shown in [27]. Moreover, we study different versions of Morse potential so as to reveal the importance of stochastic fluctuations not incorporated in other analysis tools such as linear stability analysis or deterministic PDEs which are usually trapped in local minima of the complex energy landscape.

The organization of the paper is as follows. Section 2 discusses the microscopic Ising formulation for surface diffusion as well the coarse-grained model for Metropolis and Arrhenius dynamics. Langevin approximation and mesoscopic SPDEs for both

dynamics are also presented in the same Section. In Section 3, the proposed SDE models are presented and their approximation properties are derived while in Section 4 pattern formation phenomena are observed and studied. Finally, Section 5 concludes the paper and suggests further directions of future work.

2. Background. Let us begin with the presentation of the microscopic model and continue with its coarse-grained analog. Two different dynamics namely Metropolis and Arrhenius are considered. Then the derivation of CGL approximation model is reviewed and finally the mesoscopic SPDEs which one way to be obtained is through taking the limit of the coarse-grained model [4] are given. Fig. 2.1(a) schematically depicts the position in space and time scales of the revised models while Fig. 2.1(b) shows the actual lattices of various models discussed in the following Sections. Please note that our interest in this paper lies both in microscopic and in mesoscopic scales.

2.1. Microscopic Model. Consider a finite, periodic, d-dimensional, fine lattice (left drawing in Fig. 2.1(b)) defined by $\mathcal{L}_N := \frac{1}{N}\mathbb{Z}^d \bigcap [0,1]^d$ where $\frac{1}{N}$ is the size of the lattice site while N^d is the total number of sites of the lattice. At each lattice site $x \in \mathcal{L}_N$, an order parameter –usually referred as spin– is allowed to take two values 0 describing vacant and 1 describing occupied. On the fine lattice a spin configuration is defined as $\sigma := \{\sigma(x) \in \{0,1\} : x \in \mathcal{L}_N\}$ and it is an element of the configuration space $\Sigma := \{0,1\}^{\mathcal{L}_N}$.

The energy of the system evaluated at σ is given by the Hamiltonian

$$H(\sigma) := -\frac{1}{2} \sum_{\substack{x,\, y \,\in\, \mathcal{L}_N \\ y \,\neq\, x}} J(x-y)\sigma(x)\sigma(y) + \sum_{x \in \mathcal{L}_N} h(x)\sigma(x) \tag{2.1}$$

where $J(\cdot)$ is the interaction potential between the sites while $h(\cdot)$ is the external field applied to the system. Note that the interaction potential has radial symmetry and it is appropriately scaled so as the derived mesoscopic limit is well-defined. Moreover, interaction potential has support in $[-\frac{L}{N}, \frac{L}{N}]^d$, thus, its interaction length is L sites. Equilibrium states (i.e. invariant measure) of the model at inverse temperature β is described by the Gibbs measure given by

$$\mu_{N,\beta}(d\sigma) = \frac{1}{Z_{N,\beta}} e^{-\beta H(\sigma)} P(d\sigma) \tag{2.2}$$

where $Z_{N,\beta}$ is the normalization factor that makes $\mu_{N,\beta}$ a measure while $P(d\sigma)$ is the prior measure defined as a product of independent Bernoulli random variables one for each lattice site.

Surface diffusion is simulated as spontaneous spin exchange between two neighboring sites, x, y with the restriction that every site cannot contain more than one particle (exclusion principle). Two different spin exchange dynamics which satisfy the detailed balance condition are considered. The first surface diffusion dynamics is Metropolis and its exchange rate is defined for two by neighboring sites, x, y at configuration σ as [6]

$$c(x,y,\sigma) := d_0 \exp(\beta \min\{0, (\sigma(x) - \sigma(y))(U(x,\sigma) - U(y,\sigma))\}) \tag{2.3}$$

where d_0 is the diffusion rate which depends on physical properties of the surface while $U(x,\sigma)$ is the potential of the site x given that the current configuration is σ

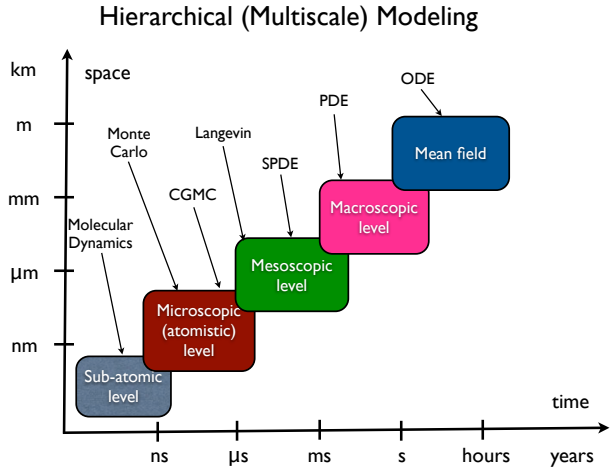

(a) Due to wide range of characteristic length scales and characteristic time scales, several models and simulation algorithms have been developed in the literature. The proposed Langevin models provide a "bridge" between the continuum models and the microscopic processes.

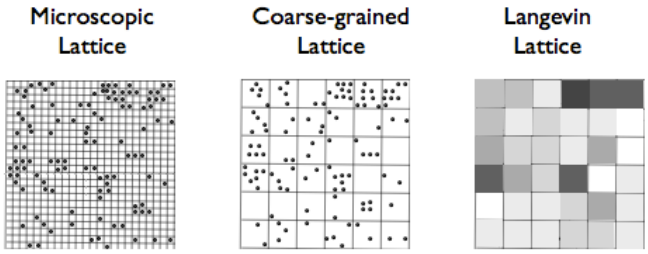

(b) Various lattices at different scales in space. Notice that both coarse-grained and Langevin lattices have the same and known spatial scale while their order parameters take discrete and continuous values, respectively.

Fig. 2.1: Hierarchical modeling at different time and space scales.

defined as

$$U(x,\sigma) := \sum_{\substack{y \in \mathcal{L}_N \\ x \neq y}} J(x-y)\sigma(y) - h(x) \tag{2.4}$$

Despite using Metropolis dynamics in many studies, a more natural and possibly more appropriate description of the finite time surface diffusion dynamics is Arrhenius dynamics. In Arrhenius dynamics, a spin exchange is performed when the activation energy is above an energy barrier which depends on the properties of the potential energy of the surface [28], [29]. Arrhenius dynamics for spin exchange (surface diffusion)

between two neighboring sites, x, y is given by

$$c(x,y,\sigma) := d_0(1-\sigma(x))\sigma(y)e^{-\beta(U_0+U(x,\sigma))} + d_0\sigma(x)(1-\sigma(y))e^{-\beta(U_0+U(y,\sigma))} \quad (2.5)$$

where d_0 and U_0 are the diffusion rate and the energy barrier of the surface, respectively, and depend on the physical properties of the diffusion process while $U(x,\sigma)$ is as before the potential of the site x. Thus, a continuous-time jump Markov process $\{\sigma_t\}_{t\geq 0}$ on $L^\infty(\Sigma;\mathbb{R})$ is defined with generator

$$\frac{d}{dt}\mathbb{E}[f(\sigma_t)|\sigma] = \mathcal{L}f(\sigma) = \sum_{\substack{x,\, y\, \in\, \mathcal{L}_N \\ x\, \neq\, y}} c(x,y,\sigma)\Big(f(\sigma^{(x,y)}) - f(\sigma)\Big) \quad (2.6)$$

for any test function $f \in L^\infty(\Sigma;\mathbb{R})$. Please note that $\sigma^{(x,y)}$ denotes the new configuration of the lattice after one spin exchange between neighboring sites x and y while test function f also called observable is typically independent of the size of the lattice. A special class of observables called mesoscopic plays a crucial role in the proofs of the approximation theorems in [7], [30].

2.2. Coarse-Grained (GC) Model. The coarse-graining of the microscopic system is performed by grouping the sites of the microscopic lattice into cells. Each cell is denoted as C_k with size $|C_k| = q^d$ where q is the coarsening factor at each dimension while $k \in \mathcal{L}_m$ where $\mathcal{L}_m := \frac{1}{m}\mathbb{Z}^d \bigcap [0,1]^d$ is the CG lattice (middle drawing in Fig. 2.1(b)). Obviously, the size of the CG lattice is m^d with $m = N/q$. On the CG lattice, $\mathcal{L}_m$, a CG variable is defined for the kth cell by

$$\eta_t(k) := \sum_{x\in C_k} \sigma_t(x), \qquad k \in \mathcal{L}_m \quad (2.7)$$

thus a new continuous-time jump Markov process $\{\eta_t\}_{t\geq 0}$ is defined. In what follows, our primal interest is concentrated on the averaged coarse-grained variables defined as

$$\bar{\eta}_t(k) := \frac{\eta_t(k)}{q^d}, \qquad k \in \mathcal{L}_m \quad (2.8)$$

which are elements of the configuration space $\bar{\mathcal{H}}_{q,m} = \{0, \frac{1}{q^d}, ..., 1\}^{\mathcal{L}_m}$.

As in the microscopic formulation, averaged CG process has Hamiltonian, potential, rate (dynamics) and invariant measure which are approximations of the respective microscopic quantities. The Hamiltonian of the averaged CG process is given by

$$\bar{H}(\bar{\eta}) := -\frac{q^d}{2}\sum_{k,l\in\mathcal{L}_m} \bar{J}(k-l)\bar{\eta}_k\bar{\eta}_l + \sum_{k\in\mathcal{L}_m}(\bar{h}(k) + \frac{\bar{J}(0)}{2})\bar{\eta}_k \quad (2.9)$$

where $\bar{J}(\cdot)$ is the coarse-grained interaction potential given by

$$\bar{J}(k-l) := \begin{cases} \frac{1}{q^{2d}}\sum_{x\in C_0}^{y\in C_{k-l}} J(x-y) & \text{for } \ k \neq l \\ \frac{1}{q^d(q^d-1)}\sum_{x,y\in C_0}^{y\neq x} J(x-y) & \text{for } \ k = l \end{cases} \quad (2.10)$$

Equilibrium states of the averaged CG variables at inverse temperature β has invariant measure given by

$$\mu_{q,m,\beta}(d\bar{\eta}) = \frac{1}{Z_{q,m,\beta}} e^{-q^d\beta\bar{H}(\bar{\eta})} P_{q,m}(d\bar{\eta}) \quad (2.11)$$

where $Z_{q,m,\beta}$ is the normalization factor that makes $\mu(d\bar{\eta})_{q,m,\beta}$ a measure while $P_{q,m}(d\bar{\eta})$ is the prior measure defined as a product of binomial random variables one for each coarse cell.

The rate of the averaged CG process to jump a particle from a cell k to a neighboring cell l, denoted by $\bar{c}_{k,l}(\bar{\eta})$, is given for Metropolis dynamics by [5]

$$\bar{c}_{k,l}(\bar{\eta}) := d_0 q^d \bar{\eta}_k(1-\bar{\eta}_l)\exp\left(\beta \min\{0, \bar{U}(l,\bar{\eta}) - \bar{U}(k,\bar{\eta})\}\right) \tag{2.12}$$

where

$$\bar{U}(k,\bar{\eta}) := q^d \sum_{l\in\mathcal{L}_m} \bar{J}(k-l)\bar{\eta}(l) - (\bar{h}(k) + \bar{J}(0)) \tag{2.13}$$

is the CG potential of the kth cell. On the other hand, the exchange rate of a particle between two neighboring cells k, l is given for Arrhenius dynamics by [5]

$$\bar{c}_{k,l}(\bar{\eta}) := d_0 q^d \bar{\eta}_k(1-\bar{\eta}_l)e^{-\beta(U_0+\bar{U}(k,\bar{\eta}))} \tag{2.14}$$

Thus, the generator of the averaged CG variables, $\{\bar{\eta}_t\}_{t\geq 0}$, is

$$\frac{d}{dt}\mathbb{E}[f(\bar{\eta}_t)|\bar{\eta}] = \bar{\mathcal{L}}f(\bar{\eta}) = \sum_{k,l\in\mathcal{L}_m} \bar{c}_{k,l}(\bar{\eta})(f(\bar{\eta} + \frac{1}{q^d}(\delta_l(k) - \delta_k(l))) - f(\bar{\eta})) \tag{2.15}$$

for any test function $f \in L^\infty(\bar{\mathcal{H}}_{q,m};\mathbb{R})$.

Finally, the weak error analysis between the microscopic process and the CG process performed in [7] uses consistency with the backward Kolmogorov equation

$$\begin{aligned} \partial_t w + \bar{\mathcal{L}}w = 0\ , \qquad t < T \\ w(\cdot, T) = f \end{aligned} \tag{2.16}$$

which corresponds to the master equation for expected values $w(z,t) = \mathbb{E}[f(\bar{\eta}_T)|\bar{\eta}_t = z]$. Thus, using observables with bounded derivatives and Kolmogorov consistency, it was rigorously shown that the weak error between the microscopic process and the CG process is of order $O((\frac{q^d}{L})^2)$ which is affordable for mid and long range interaction potentials ($L >> 1$).

Remark: The computational acceleration of the CGMC algorithm for simulating surface diffusion processes stems not only from the reduced number of parameters by a factor of q^d but also from the time acceleration by a factor of q^{2d} [6]. Intuitively, the time-acceleration can be understood by the fact that one event in the CG simulation is the jump of a particle from a cell to a neighborhood cell while in microscopic simulation the same event can be a (possibly long) sequence of jumps.

2.3. Coarse-Grained Langevin (CGL) Approximation. Generally in Langevin methods, the microscopic process is approximated by a process driven by a system of SDEs [18], [31]. For surface diffusion particularly, Langevin approximation for the coarse-grained model was recently derived in [20]. Concentrating for notational simplicity in 1D, the CG Langevin SDE system is given by

$$d\tilde{\eta}_k = a_k(\tilde{\eta})dt + \sum_{l\in\mathcal{L}_m} b_{k,l}(\tilde{\eta})dW_l, \qquad k \in \mathcal{L}_m \tag{2.17}$$

where $\tilde{\eta} = \{\tilde{\eta}_k : k \in \mathcal{L}_m\}$ is the SDE process set on the configuration space $\tilde{\mathcal{H}}_{q,m} = [0,1]^{\mathcal{L}_m}$ (see right drawing in Fig. 2.1(b)) while $a(\tilde{\eta}) = \{a_k(\tilde{\eta}) : k \in \mathcal{L}_m\}$ and $b(\tilde{\eta}) =$

$\{b_{k,l}(\tilde{\eta}) : k, l \in \mathcal{L}_m\}$ are the drift vector and the diffusion matrix of the SDE process, respectively. The generator of this process is defined for an arbitrary test function $f \in L^\infty(\tilde{\mathcal{H}}_{q,m}; \mathbb{R})$ as

$$\frac{d}{dt}\mathbb{E}[f(\tilde{\eta}_t)|\tilde{\eta}] = \tilde{\mathcal{L}}f(\tilde{\eta}) = \sum_{k\in\mathcal{L}_m} a_k(\tilde{\eta})\frac{\partial f}{\partial \tilde{\eta}_k} + \frac{1}{2}\sum_{k,l\in\mathcal{L}_m}(bb^T)_{kl}(\tilde{\eta})\frac{\partial^2 f}{\partial\tilde{\eta}_k\partial\tilde{\eta}_l} \tag{2.18}$$

In order to estimate the drift and diffusion terms, the weak global error between the CG process and CGL process is minimized. Thus, defining for a mesoscopic observable[1], f, the expected value $w(z,t) = \mathbb{E}[f(\tilde{\eta}_T)|\tilde{\eta}_t = z]$, weak error is written as

$$\begin{aligned}
&\mathbb{E}[f(\bar{\eta}_T)] - \mathbb{E}[f(\tilde{\eta}_T)] = \mathbb{E}[\mathbb{E}[f(\tilde{\eta}_T)|\tilde{\eta}_T = \bar{\eta}_T]] - \mathbb{E}[\mathbb{E}[f(\tilde{\eta}_T)|\tilde{\eta}_0 = \bar{\eta}_0]] = \\
&\mathbb{E}[w(\bar{\eta}_T, T)] - \mathbb{E}[w(\bar{\eta}_0, 0)] = \int_0^T \mathbb{E}[\bar{\mathcal{L}}w(\bar{\eta}) + \partial_t w(\bar{\eta})]dt = \\
&\int_0^T \mathbb{E}[\bar{\mathcal{L}}w(\bar{\eta}) - \tilde{\mathcal{L}}w(\bar{\eta})]dt = \int_0^T \mathbb{E}[e_{loc}(w)]dt
\end{aligned} \tag{2.19}$$

where the third equation is the martingale property while the fourth one uses the backward equation for $\tilde{\mathcal{L}}$ [30]. Moreover, according to (2.19), the local error for a mesoscopic observable f, $e_{loc}(f)$, can be defined on the difference of the generators of the two processes as

$$\begin{aligned}
e_{loc}(f) &= \bar{\mathcal{L}}f(\bar{\eta}) - \tilde{\mathcal{L}}f(\bar{\eta}) \\
&= \sum_{k,l\in\mathcal{L}_m} \bar{c}_{k,l}(\bar{\eta})(f(\bar{\eta} + \frac{1}{q}(\delta_l(k) - \delta_k(l))) - w(\bar{\eta})) \\
&- \sum_{k\in\mathcal{L}_m} a_k(\bar{\eta})\frac{\partial f}{\partial\bar{\eta}_k} - \frac{1}{2}\sum_{k,l\in\mathcal{L}_m}(bb^T)_{kl}(\bar{\eta})\frac{\partial^2 f}{\partial\bar{\eta}_k\partial\bar{\eta}_l}
\end{aligned} \tag{2.20}$$

2.3.1. Weak Error Analysis. By applying Taylor series expansion for $f(\bar{\eta} + \frac{1}{q}(\delta_l(k) - \delta_k(l)))$ and appropriately choosing the drift and diffusion terms so as to eliminate the first and second order of the expansion, it was obtained in [20] that the kth element of the drift vector is

$$a_k(\tilde{\eta}) = \frac{1}{q}[\bar{c}_{k+1,k}(\tilde{\eta}) - \bar{c}_{k,k+1}(\tilde{\eta}) + \bar{c}_{k-1,k}(\tilde{\eta}) - \bar{c}_{k,k-1}(\tilde{\eta})] \tag{2.21}$$

while the non-zero elements of the diffusion matrix are

$$\begin{aligned}
b_{k,k}(\tilde{\eta}) &= \frac{1}{q}\sqrt{\bar{c}_{k+1,k}(\tilde{\eta}) + \bar{c}_{k,k+1}(\tilde{\eta})} \\
b_{k+1,k}(\tilde{\eta}) &= -b_{k,k}(\tilde{\eta})
\end{aligned} \tag{2.22}$$

Thus the formal local error between CG process and CGL approximation process is

$$e_{loc}(w) = O(\frac{1}{q^3}) \times O(\bar{c}_{k,l}) = O(\frac{1}{q^2}) \tag{2.23}$$

[1] A mesoscopic observable is a function whose derivatives –in this particular case up to third order [30]– are bounded and the bounds are independent of the dimension (i.e. the size of the CG lattice).

Therefore, based on the above approximation, finite time global weak error between CG process and its CGL approximation could be rigorously obtained for mesoscopic observables by using again Kolmogorov consistency of the backward equation and Bernstein-type bound estimates for the derivatives of $w(z,t)$. Indeed, it was shown in [30] that the weak error for mesoscopic observables is

$$\mathbb{E}[f(\bar{\eta}_T)] - \mathbb{E}[f(\tilde{\eta}_T)] = O(\frac{1}{q^2}) \tag{2.24}$$

when absorption/desorption processes were considered and we expect the same result is true for diffusion processes.

2.4. Mesoscopic SPDE Limit and LDP. In this Section, we review mesoscopic evolution equations arising in surface processes derived from the microscopic stochastic models presented above. In general there are two families of mesoscopic equations depending on the presence of stochasticity. Here we concentrate on the stochastic integro-differential equations for Metropolis and Arrhenius dynamics. Both dynamics can be written as a constrained gradient flow equation plus a multiplicative stochastic term with different mobilities. Indeed, the unified stochastic mass-conserved equation (SPDE) is given formally by [11], [15]

$$\partial_t \rho = \nabla \cdot \left\{ L[\rho] \nabla \frac{\delta E}{\delta \rho} \right\} + \frac{1}{\sqrt{N^d}} \nabla \cdot \left\{ \sqrt{2L[\rho]} \dot{W} \right\} \tag{2.25}$$

where $\rho(x,t)$ is the zero lattice-size limit of the empirical measure of the particles which evolves slowly similar to a density while $E[\cdot]$ is the Lyapunov functional (free energy functional) of the deterministic mesoscopic equation given by

$$E[\rho] = -\frac{\beta}{2} \int \int J(x-x')\rho(x)\rho(x')dxdx' + \beta \int h(x)\rho(x)dx + \int R(\rho(x))dx \tag{2.26}$$

where $J(\cdot)$ and $h(\cdot)$ are continuous versions of the interaction potential and external field, respectively, while $R(\cdot)$ is the entropy of the system given by

$$R(\rho) = \rho \log(\rho) + (1-\rho)\log(1-\rho) \tag{2.27}$$

$L[\rho]$ is the mobility of the equation which determines the dynamics of the system while $\dot{W}(x,t)$ is space-time white noise. The invariant measure for the equilibrium states of the solution of (2.25) is given formally by [2]

$$\mu_N(d\rho) = \frac{1}{Z_N} e^{-N^d E(\rho)} d\rho \tag{2.28}$$

A formal approach to derive the above invariant measure is to take the zero lattice-size limit of the CG invariant measure given by (2.11). Indeed, another way to write down (2.11) is to expand the binomial prior distribution using Sterling's formula [4]. Then the invariant measure is written as

$$\mu_{q,m,\beta}(d\bar{\eta}) = \frac{1}{Z_{q,m,\beta}} e^{-q^d m^d (\bar{E}(\bar{\eta}) + \frac{1}{2q^d}\bar{G}(\bar{\eta}) + O(\frac{1}{q^{2d}}))} \tag{2.29}$$

where

$$\bar{E}(\bar{\eta}) = \frac{1}{m^d}[\beta \bar{H}(\bar{\eta}) + \bar{R}(\bar{\eta})] \tag{2.30}$$

is a discrete version of the Lyapunov functional while $\bar{H}(\cdot)$ and $\bar{R}(\cdot)$ are the Hamiltonian in (2.9) and the discrete entropy of the system (i.e. $\bar{R}(\bar{\eta}) = \sum_{k\in\mathcal{L}_m}[\bar{\eta}_k \log(\bar{\eta}_k) + (1-\bar{\eta}_k)\log(1-\bar{\eta}_k)]$), respectively. The additional term in (2.29) is the primal remainder of the Sterling's expansion which equals to $\bar{G}(\bar{\eta}) = \frac{1}{m^d}\sum_{k\in\mathcal{L}_m} \log(\bar{\eta}_k(1-\bar{\eta}_k))$. Notice that the additional term, $\bar{G}(\cdot)$, may be significant when coarsening factor, q, takes small values, however, in the zero lattice-size limit the only term that survives is the Lyapunov functional, $\bar{E}(\cdot)$.

The mobility for Metropolis dynamics equals to $L[\rho] = d_0\rho(1-\rho)$, thus, the SPDE for Metropolis dynamics is given by

$$\partial_t\rho = \nabla\cdot\{d_0(\nabla\rho - \beta\rho(1-\rho)\nabla(J*\rho))\} + \frac{1}{\sqrt{N^d}}\nabla\cdot\left\{\sqrt{2d_0\rho(1-\rho)}\dot{W}\right\} \tag{2.31}$$

where $*$ denotes convolution. For Arrhenius dynamics, the mobility is more complex and it is given by $L[\rho] = d_0\rho(1-\rho)\exp(-\beta(U_0 + J*\rho))$, thus, the mesoscopic SPDE for this case is

$$\begin{aligned}\partial_t\rho = {}& \nabla\cdot\{d_\beta\exp(-\beta J*\rho)(\nabla\rho - \beta\rho(1-\rho)\nabla(J*\rho))\} \\ & + \frac{1}{\sqrt{N^d}}\nabla\cdot\left\{\sqrt{2d_\beta\rho(1-\rho)\exp(-\beta J*\rho)}\dot{W}\right\}\end{aligned} \tag{2.32}$$

where $d_\beta = d_0 e^{-\beta U_0}$.

Finally, SPDEs such as (2.25) are generally ill-behaved mathematical objects especially in high dimensions and they are usually treated in a formal way as here. Nevertheless, an indirect yet rigorous analysis could be carried out for SPDEs using the theory of Large Deviations (LD) [32]. Indeed, SPDE (2.25) is related with the action functional for the microscopic process obtained by taking the hydrodynamic limit. For exchange dynamics with exclusion principle and long range interaction potential, it was shown in [33] that the action functional for an absolutely continuous function $\Psi : [0,1]^d \times [0,T] \to \mathbb{R}$ equals to

$$S_{0T}(\Psi) = \int_0^T\int_0^1 L[\Psi](\nabla H)^2 dxdt \tag{2.33}$$

where H solves

$$\partial_t\Psi = \nabla\cdot\left\{L[\Psi](\frac{\nabla\Psi}{\Psi(1-\Psi)} - \beta\nabla(J*\Psi + h))\right\} + 2\nabla\cdot\{L[\Psi]\nabla H\} \tag{2.34}$$

which is the second order backward PDE of (2.25). Intuitively, the action functional $S_{0T}(\Psi)$ assigns a probability to the event ρ that follows the path Ψ which can be formally stated by the following asymptotic formula

$$P\{\nu(\rho,\Psi) \le \delta\} \sim e^{-N^{-d}S_{0T}(\Psi)} \tag{2.35}$$

for suitably chosen $\delta, \epsilon > 0$ where ν is a metric in a proper function space that measures the distance between ρ and Ψ. Further details on LD theory can be found in Section 3.4.

Remark: Even though, mesoscopic models –either deterministic or stochastic– are computationally tractable compared to microscopic or even CG models they lack of some interesting properties. For instance, due to the limiting process, the actual length-scale of the system is not obvious. Moreover, the space discretization is not a trivial issue especially for the stochastic case since the properties of the discrete and the continuous models may be totally different. These facts will be highlighted in the following Sections.

3. Langevin-type Approximation Models. As it was reviewed in Section 2.3, classical Langevin models are derived as approximations of the atomistic processes by formally minimizing the local error between the microscopic process and the SDE process. In connection with Fig. 2.1(a), Langevin approximation is an approach which translates the atomistic processes from the microscopic level to the coarser mesoscopic level. In this Section, we proceed in the opposite direction (i.e. from mesoscopic to microscopic level) and derive three Langevin-type models from mesoscopic equations for the simulation of surface diffusion processes which additionally to the properties of the classical Langevin approximation they satisfy – actually two of them– detailed balance condition (DBC). Eventually, our goal is to control the error of the derived approximations at three different time-scales which are

a. Finite times through weak error estimates between the microscopic process and the derived models.
b. Long times and phase transitions through LD theory and asymptotic equivalence of the rate (action) functionals.
c. Infinite times through the knowledge of the invariant measure of the derived approximation process.

To begin, the first proposed model is a 2nd order space discretization of the mesoscopic SPDE. We refer to it as Direct Langevin approximation model (DLM) because the local error between DLM and CGL of [20] is of order $O(\frac{1}{m^2})$ for the drift term while it is of order $O(\frac{1}{qm})$ for the diffusion term (see Section 3.1.1) which are considered negligible. Yet, as in CGL approximation, the DBC is not satisfied for DLM thus the invariant measure of the stochastic process is not known. By adding a "correction" term to the drift, the second model referred to as perturbed Langevin approximation model 1 (PLM1) is defined. For this variant, DBC is satisfied and the invariant measure is a discrete version of the continuous invariant measure given by (2.28). However, the finite time dynamics of PLM1 are perturbed due to the additional "correction" term. The third model referred to as PLM2 tries to overcome the induced error at the dynamics by adding a perturbation term to the invariant measure. An appropriate choice of the perturbation term leads to the elimination of the "correction" term of PLM1 restoring the accuracy of the finite time dynamics. Table 3.1 summarizes the properties of CGL approximation as well the properties of the three proposed models which we will derive in the remaining of this Section.

	Weak Error of order $O(\frac{1}{q^{2d}})$	LD Theory	Invariant Measure
CGL	Yes	Yes	No
DLM	Yes	Yes	No
PLM1	No	Yes	Yes
PLM2	Yes	Yes	Yes

Table 3.1: Summary of the properties of the derived diffusion models at different time scales. Note that for adsorption/desorption processes the answer to the LD Theory column is 'No' [34], [20].

Before starting presenting the proposed models, we make the following simplifications. Without loss of generality we concentrate on the 1D case. We revisit the general d-dimensional case in Section 4 where the details of the numerical implementation are given. Moreover, external field is assumed to be zero without this being a restriction to the final outcome.

3.1. Direct Langevin Approximation Model (DLM). The first approximation model is a straightforward second-order, finite-difference, mass-conserved space-discretization of the mesoscopic SPDE. The discretized density vector is denoted by $\rho = \{\rho_k : k \in \mathcal{L}_m\}$. Then for the kth density element, a stochastic differential equation is defined by

$$d\rho_k = u_k(\rho)dt + \sum_{l\in\mathcal{L}_m} v_{k,l}(\rho)dW_l, \qquad k \in \mathcal{L}_m \tag{3.1}$$

where

$$u_k(\rho) = \frac{1}{2}(L_{k+1}(\rho) + L_k(\rho))\left[\frac{\partial\bar{E}(\rho)}{\partial\rho_{k+1}} - \frac{\partial\bar{E}(\rho)}{\partial\rho_k}\right]dt - \frac{1}{2}(L_k(\rho) + L_{k-1}(\rho))\left[\frac{\partial\bar{E}(\rho)}{\partial\rho_k} - \frac{\partial\bar{E}(\rho)}{\partial\rho_{k-1}}\right] \tag{3.2}$$

is the kth element of the drift vector. Note that $\bar{E}(\rho)$ is the discrete free energy functional given by (2.30) while $L_k(\rho)$ is the discrete version of the mobility. For Metropolis dynamics, the mobility is given by

$$L_k(\rho) = d_0\rho_k(1-\rho_k) \quad , \tag{3.3}$$

which depends only on the kth density parameter ρ_k while the mobility for Arrhenius dynamics is given by

$$L_k(\rho) = d_\beta\rho_k(1-\rho_k)e^{-\beta\bar{U}(k,\rho)} \quad , \tag{3.4}$$

which depends not only on ρ_k but also on the neighboring density variables through the potential $\bar{U}(k,\rho)$. The non-zero elements of the diffusion matrix are

$$\begin{aligned} v_{k,k}(\rho) &= \sqrt{\frac{1}{q}(L_{k+1}(\rho) + L_k(\rho))} \quad , \\ v_{k+1,k}(\rho) &= -v_{k,k}(\rho) \ . \end{aligned} \tag{3.5}$$

Hence the covariance matrix (i.e. square matrix of the diffusion matrix) is a tridiagonal matrix with non-zero elements

$$\begin{aligned} (vv^T)_{k,k}(\rho) &= \frac{1}{q}[L_{k+1}(\rho) + L_{k-1}(\rho) + 2L_k(\rho)] \quad , \\ (vv^T)_{k\pm1,k}(\rho) &= -\frac{1}{q}[L_{k\pm1}(\rho) + L_k(\rho)] \ . \end{aligned} \tag{3.6}$$

It is noteworthy that the scaling of the noise in (3.5) is $\frac{1}{\sqrt{q}}$ which is different from the scaling $\frac{1}{\sqrt{qm}}$ of the mesoscopic SPDE (2.25). The reason is that in order to relate the process generated from (3.1) with the CG process or the CGL process (i.e $\rho_k \approx \tilde{\eta}_k \approx \bar{\eta}_k$) the appropriate scaling for the stochastic term is $\frac{1}{\sqrt{q}}$ as the following subsection reveals. Linked with Fig. 2.1(a), different scalings of the noise result in models with different positions at the mesoscopic level. Typically, when zooming into the atomistic details is performed, the power of the noise is increased while when zoom out is performed the noise is faded out.

Additionally, the existence of a Lyapunov functional is usually crucial for the study of an (S)PDE either theoretically or numerically. In (3.1), if the noise is cancelled out then $\bar{E}(\rho)$ is a discrete Lyapunov functional since it is decreasing over time (see Appendix B). Of course, when noise is present Lyapunov functional may increase due to stochastic fluctuations nevertheless on average it decreases. Next we proceed with the properties that relates the process driven by (3.1) with the CG and CGL processes.

3.1.1. Weak Error Analysis. The estimation of the finite-time weak error between the DLM process, ρ_t, and the CG process, $\bar{\eta}_t$, uses as an auxiliary intermediate step the CGL process, $\tilde{\eta}_t$. Indeed, the weak error for a suitable mesoscopic observable, f, can be written as

$$\mathbb{E}[f(\bar{\eta}_T)] - \mathbb{E}[f(\rho_T)] = \mathbb{E}[f(\bar{\eta}_T)] - \mathbb{E}[f(\tilde{\eta}_T)] + \mathbb{E}[f(\tilde{\eta}_T)] - \mathbb{E}[f(\rho_T)] \tag{3.7}$$

and at least formally it was shown in [20] and briefly reviewed in Section 2.3 that $\mathbb{E}[f(\bar{\eta}_T)] - \mathbb{E}[f(\tilde{\eta}_T)] = O(\frac{1}{q^2})$. On the other hand, the local error between the CGL process and the DLM process defined in (3.1) is given by

$$\tilde{\mathcal{L}}f(\rho) - \mathcal{M}f(\rho) = \sum_{k\in\mathcal{L}_m} [a_k(\rho) - u_k(\rho)]\frac{\partial f}{\partial \rho_k} - \frac{1}{2}\sum_{k,l\in\mathcal{L}_m} [(bb^T)_{kl}(\rho) - (vv^T)_{kl}(\rho)]\frac{\partial^2 f}{\partial\rho_k\partial\rho_l} \tag{3.8}$$

where $\mathcal{M}$ is the generator of the process driven by (3.1) given by

$$\mathcal{M}f(\rho) = \sum_{k\in\mathcal{L}_m} u_k(\rho)\frac{\partial f}{\partial \rho_k} + \frac{1}{2}\sum_{k,l\in\mathcal{L}_m} (vv^T)_{kl}(\rho)\frac{\partial^2 f}{\partial\rho_k\partial\rho_l} \tag{3.9}$$

for any test function $f \in L^\infty(\tilde{\mathcal{H}}_{q,m};\mathbb{R})$.

It is straightforward to compute (see Appendix A) that the drift term has the following formal asymptotic expansion

$$u_k(\rho) = \frac{1}{m^2}\partial_x\left\{L_k(\rho)\left[\frac{\partial_x\rho(x_k)}{\rho(x_k)(1-\rho(x_k))} - \beta\partial_x\bar{U}(k,\rho)\right]\right\} + O(\frac{1}{m^4}) \tag{3.10}$$

where $\rho(x_k) = \rho(x_k,t)$ is the continuous space density function at position $x_k = \frac{k}{m}$, $k = 0,...,m-1$ and it should not be confused with the DLM process, ρ_k, which is discrete in space. Similarly, the weak asymptotic formula for the covariance matrix of the diffusion for two test functions $\phi_1(x)$ and $\phi_2(x)$ is given by

$$\begin{aligned}&\left\langle \sum_{k,j} v^T_{j,k}(\rho)\phi_1(x_j)\frac{dW_k}{dt}, \sum_{l,i} v^T_{i,l}(\rho)\phi_2(x_i)\frac{dW_l}{dt}\right\rangle \\ &= \frac{2}{qm}\int L[\rho(x)]\partial_x\phi_1(x)\partial_x\phi_2(x)dx + O(\frac{1}{m^4})\end{aligned} \tag{3.11}$$

The same asymptotic expressions have been derived for CGL approximation in [20]. Moreover, applying the time rescaling $t \to m^2 t$ suggested by the above asymptotics to both DLM and CGL processes, it is allowed to formally write that

$$u_k(\tilde{\eta}) = a_k(\tilde{\eta}) + O(\frac{1}{m^2}) \tag{3.12}$$

where $a(\cdot)$ is the drift vector of the CGL process given by (2.21). Similarly, having in mind that Brownian motion scales as $W_{m^2 t} = \frac{1}{m}W_t$, it is straightforward to show that

$$\begin{aligned}(vv^T)_{k,k}(\tilde{\eta}) &= (bb^T)_{k,k}(\tilde{\eta}) + O(\frac{1}{qm}) \\ (vv^T)_{k\pm1,k}(\tilde{\eta}) &= (bb^T)_{k\pm1,k}(\tilde{\eta}) + O(\frac{1}{qm})\end{aligned} \tag{3.13}$$

where $b(\cdot)$ is the diffusion matrix of the CGL process. Thus substituting (3.12) and (3.13) into (3.8) we derive at least formally that

$$\tilde{\mathcal{L}}f(\rho) - \mathcal{M}f(\rho) = O(\frac{1}{qm}) \tag{3.14}$$

and using the same arguments presented in [30] and briefly reviewed in Section 2.3, the weak error could be rigorously proved to have the same $O(\frac{1}{qm})$ order of error. Finally, notice that $q << m$ hence the weak error between the CG process and the DLM process is of order $O(\frac{1}{q^2})$.

3.1.2. Is DBC satisfied? A guess for the invariant measure of the DLM process could be

$$\mu(d\rho) = \frac{1}{Z} e^{-q\bar{E}(\rho)} \prod_{k\in\mathcal{L}_m} d\rho_k \tag{3.15}$$

which is a discrete version of (2.28). However, this guess is not correct because the operator $\mathcal{M}$ (i.e. the generator) is not self-adjoint ($\mathcal{M} \neq \mathcal{M}^*$) with respect to the measure μ. Indeed, we compute (see Appendix B) that

$$< \mathcal{M}f, g >_{L^2(\mu)} = < f, \mathcal{M}g >_{L^2(\mu)} - \frac{1}{2q} \int \sum_{k\in\mathcal{L}_m} C_k(\rho) \left[\frac{\partial g}{\partial \rho_k} f - \frac{\partial f}{\partial \rho_k} g \right] \mu(d\rho) \tag{3.16}$$

where $< \cdot, \cdot >_{L^2(\mu)}$ denotes the inner product between two functions with respect to measure μ while

$$C_k(\rho) = \left[\frac{\partial L_{k+1}}{\partial \rho_k} + \frac{\partial L_{k-1}}{\partial \rho_k} + 2\frac{\partial L_k}{\partial \rho_k} - \frac{\partial L_{k+1}}{\partial \rho_{k+1}} - \frac{\partial L_k}{\partial \rho_{k+1}} - \frac{\partial L_k}{\partial \rho_{k-1}} - \frac{\partial L_{k-1}}{\partial \rho_{k-1}} \right] \tag{3.17}$$

is an interference term which depends only on the mobility of the process.
Remark: For the case where the mobility is constant (additive noise) or even linear then $C_k(\rho) = 0$ for all k thus DBC is satisfied and $\mu(d\rho)$ is the invariant measure of the process. However, the mobility of both Metropolis and Arrhenius dynamics which partially reflects the exclusion principle of the microscopic process are more complex hence the invariant measure is not known explicitly.

3.2. Perturbed Langevin Model 1: Satisfying the DBC. The second approximation model (PLM1) is obtained by adding a "correction" term to the drift which cancels the interference term in (3.16). Thus, the kth element of the density vector of PLM1 is given by

$$d\bar{\rho}_k = \left(u_k(\bar{\rho}) + \frac{1}{2q} C_k(\bar{\rho}) \right) dt + \sum_{l\in\mathcal{L}_m} v_{k,l}(\bar{\rho}) dW_l, \qquad k \in \mathcal{L}_m \tag{3.18}$$

which is obtained from DML with a perturbation of order $O(\frac{1}{q})$ to the drift.

PROPOSITION 3.1. *The stochastic process driven by (3.18) satisfies the DBC and its invariant measure is $\mu(d\bar{\rho})$ given in (3.15).*

Proof. The generator of the new process denoted by $\bar{\mathcal{M}}$ is written for a test function f as

$$\bar{\mathcal{M}}f(\bar{\rho}) = \mathcal{M}f(\bar{\rho}) + \frac{1}{2q} \sum_{k\in\mathcal{L}_m} C_k(\bar{\rho}) \frac{\partial f}{\partial \bar{\rho}_k} \tag{3.19}$$

hence using (3.16) which has been derived in Appendix B it is straightforward to show that

$$< \bar{\mathcal{M}} f, g >_{L^2(\mu)} = < f, \bar{\mathcal{M}} g >_{L^2(\mu)} \tag{3.20}$$

□

3.2.1. Weak Error Analysis. Due to the "correction" term added to the drift, the finite time dynamics of PLM1 are perturbed. Indeed, the local error between the PLM1 process and the DLM process for a test function f, which is defined as the difference of the two processes' generators (see Section 2.3), is

$$\mathcal{M} f(\rho) - \bar{\mathcal{M}} f(\rho) = \sum_{k \in \mathcal{L}_m} C_k \frac{\partial f}{\partial \rho_k} = O(\frac{1}{q}) \tag{3.21}$$

Hence, the weak error between the CG process and the PLM1 process is expected to be of order $O(\frac{1}{q})$ which is worse than the weak error between the CG process and the DML process. Overall, the cost paid for constructing a model with known invariant measure is to introduce error at finite times. Thus, in order to gain better understanding of the induced error, lets compute explicitly as well asymptotically the added "correction" term.

3.2.2. "Correction" Term Asymptotics. For Metropolis dynamics, the "correction" term is twice the discrete Laplacian of the density thus its asymptotic is given by

$$C_k(\rho) = 2[\rho_{k+1} + \rho_{k-1} - 2\rho_k] = \frac{2}{m^2} \partial_{xx} \rho(x_k) + O(\frac{1}{m^4}) \tag{3.22}$$

Interestingly, the Laplacian of the density is also obtained asymptotically from the entropy term of the free energy functional (see (2.31)). Similarly, the "correction" term for the more complex Arrhenius dynamics is given by

$$\begin{aligned} C_k(\rho) &= 2\left(\frac{1-2\rho_k}{\rho_k(1-\rho_k)} - \beta(\bar{J}(0)+\bar{J}(1))\right) L_k(\rho) \\ &- \left(\frac{1-2\rho_{k+1}}{\rho_{k+1}(1-\rho_{k+1})} - \beta(\bar{J}(0)+\bar{J}(1))\right) L_{k+1}(\rho) - \left(\frac{1-2\rho_{k-1}}{\rho_{k-1}(1-\rho_{k-1})} - \beta(\bar{J}(0)+\bar{J}(1))\right) L_{k-1}(\rho) \\ &= -\frac{1}{m^2}\partial_{xx}\left\{\left(\frac{1-2\rho(x_k)}{\rho(x_k)(1-\rho(x_k))} - \beta(\bar{J}(0)+\bar{J}(1))\right) L_k(\rho)\right\} + O(\frac{1}{m^4}) \end{aligned} \tag{3.23}$$

where the last equation is its asymptotic expansion. However another less accurate yet more manageable asymptotic expansion for the Arrhenius "correction" term is needed which is given by (see Appendix A)

$$\begin{aligned} C_k(\rho) = \frac{\partial_x}{m^2}\Big\{ &\frac{2\partial_x \rho(x_k)}{\rho(x_k)(1-\rho(x_k))} L_k(\rho) + \beta^2(\bar{J}(0)+\bar{J}(1))\partial_x \bar{U}(k,\rho) L_k(\rho) \\ &+ \beta\gamma \frac{(1-2\rho(x_k))\partial_x \rho(x_k)}{\rho(x_k)(1-\rho(x_k))} L_k(\rho)\Big\} + O(\frac{L^2}{q^2 m^4}) \end{aligned} \tag{3.24}$$

where $\gamma = (\sum_{l \neq 0,1} \bar{J}(l))$ is a constant.

3.3. Perturbed Langevin Model 2: Perturbing the invariant measure. Previous subsection motivates us to suggest a second variant of DLM with perturbed invariant measure which is able to eliminate the "correction" term from the drift. Hence, the price to be paid for correcting the finite time dynamics is a controlled-error approximation of the invariant measure. To proceed, the third approximation model (PLM2) is derived by assuming that the invariant measure of the DLM process is a perturbed version of $\mu(d\rho)$. Indeed, assuming that the (perturbed) invariant measure is given by

$$\tilde{\mu}(d\rho) = \frac{1}{\tilde{Z}} e^{-q(\bar{E}(\rho)+\frac{1}{q}\bar{P}(\rho))} \prod_{k\in\mathcal{L}_m} d\rho_k \tag{3.25}$$

where $\bar{P}(\cdot)$ is a function to be specified, then, the following computation similar to (3.16) is obtained for the generator $\mathcal{M}$ of DLM

$$< \mathcal{M}f, g >_{L^2(\tilde{\mu})} = < f, \mathcal{M}g >_{L^2(\tilde{\mu})} + \frac{1}{2q} \int \sum_{k\in\mathcal{L}_m} (P_k(\rho) - C_k(\rho)) \left[\frac{\partial g}{\partial \rho_k} f - \frac{\partial f}{\partial \rho_k} g \right] \tilde{\mu}(d\rho) \tag{3.26}$$

where $C_k(\rho)$ is given in (3.17) while

$$\begin{aligned} P_k(\rho) &= (L_{k+1}(\rho) + L_k(\rho)) \left[\frac{\partial \bar{P}}{\partial \rho_{k+1}} - \frac{\partial \bar{P}}{\partial \rho_k} \right] - (L_k(\rho) + L_{k-1}(\rho)) \left[\frac{\partial \bar{P}}{\partial \rho_k} - \frac{\partial \bar{P}}{\partial \rho_{k-1}} \right] \\ &= \frac{2}{m^2} \partial_x \left\{ \partial_x \left\{ \frac{\partial \bar{P}}{\partial \rho(x_k)} \right\} L_k(\rho) \right\} + O(\frac{1}{m^4}) \end{aligned} \tag{3.27}$$

is the interference term due to the perturbation of the invariant measure. Then PLM2 is defined for the kth density variable by

$$d\tilde{\rho}_k = \left(u_k(\tilde{\rho}) + \frac{1}{2q} \tilde{C}_k(\tilde{\rho}) \right) dt + \sum_{l\in\mathcal{L}_m} v_{k,l}(\tilde{\rho}) dW_l, \qquad k \in \mathcal{L}_m \tag{3.28}$$

where $\tilde{C}_k(\tilde{\rho}) = C_k(\tilde{\rho}) - P_k(\tilde{\rho})$ is the new "correction" term. Similarly, to the previous model, PLM2 was an explicitly known invariant measure.

PROPOSITION 3.2. *The stochastic process driven by (3.28) satisfies the DBC and its invariant measure is $\tilde{\mu}(d\tilde{\rho})$ given in (3.25).*

The proof is omitted because it is similar to the proof for PLM1.

3.3.1. Weak Error Analysis. Choosing appropriately the perturbation term, it is possible to make $\tilde{C}_k(\rho)$ negligible, e.g. (3.30). Eliminating the "correction" term implies that the drift term is not anymore perturbed and the finite time dynamics are again as accurate as the DLM dynamics. The choice of the appropriate perturbation of the invariant measure is inspired by the asymptotic expansions of the interference term (3.17) and the invariant measure perturbation (3.27). As already stated, the asymptotic of the interference term for Metropolis dynamics is the Laplacian of the density hence a suitable choice for the perturbation term is the entropy of the system. Indeed, if we set

$$\bar{P}(\tilde{\rho}) = \sum_{k\in\mathcal{L}_m} [\tilde{\rho}_k \log(\tilde{\rho}_k) + (1-\tilde{\rho}_k)\log(1-\tilde{\rho}_k)] \tag{3.29}$$

then it is obtained asymptotically that $\tilde{C}_k(\tilde{\rho}) = O(\frac{1}{m^4})$. Hence the local error between the time rescaled DML process and the time rescaled PLM2 process for any test

function, f, is

$$\mathcal{M}f(\rho) - \tilde{\mathcal{M}}f(\rho) = O(\frac{1}{qm^2}) \tag{3.30}$$

Interestingly, the perturbation term, $\bar{P}(\tilde{\rho})$, of the invariant measure for Metropolis dynamics is the entropy of the system. This implies an increase of the temperature of the system at equilibrium from β to $\beta(1+\frac{1}{q})$! Moreover, PLM2 can be thought as a space discretization of the SPDE (2.25) since it differs from DLM, which is a straightforward space discretization of the same SPDE, by a term which has order less than the order of the discretization. Consequently, it can be stated that numerical simulations of the discretized process –possibly any discretized process– are performed at a different (of order $O(\frac{1}{q})$) temperature than they were initially designed.

For Arrhenius dynamics, the derivation of the perturbed term is more difficult since the asymptotic expansion given by (3.24) is more complicated. Nevertheless, if we set

$$\begin{aligned}\bar{P}(\rho) = &\sum_{k\in\mathcal{L}_m} [\rho_k \log(\rho_k) + (1-\rho_k)\log(1-\rho_k)] - \frac{\beta^2}{4}(\bar{J}(0)+\bar{J}(1))\bar{H}(\rho) \\ &- \frac{\beta\gamma}{2}\sum_{k\in\mathcal{L}_m} [\rho_k \log(\rho_k) - (1-\rho_k)\log(1-\rho_k)]\end{aligned} \tag{3.31}$$

then the asymptotic order of the "correction" term becomes $\tilde{C}_k(\tilde{\rho}) = O(\frac{L^2}{q^2m^4})$. Hence the local error between the DLM process and the PLM2 process for Arrhenius dynamics is given by

$$\mathcal{M}f(\rho) - \tilde{\mathcal{M}}f(\rho) = O(\frac{L^2}{q^3m^2}) \tag{3.32}$$

where L is the interaction potential length. Finally, notice that for Arrhenius dynamics both Hamiltonian and entropy terms are perturbed and there is no straightforward physical interpretation of the perturbation as there was for the Metropolis case.

Remark: Comparing the perturbations terms (3.29) for Metropolis dynamics and (3.31) for Arrhenius dynamics with the additional term $\bar{G}(\cdot)$ in the invariant measure of CG process (2.29), we observe that they have the same order, $O(\frac{1}{q})$, but the actual functions are different. Of course, this is not a surprise since the former depends on the mobility (i.e. dynamics) while the latter depends on the prior distribution of the process.

3.4. Large Deviation and Action Functional. It was shown firstly by Hanggi et al. [34] that Langevin approximation may have different behavior[2] at long times compared to the microscopic process. This is established by showing the asymptotic non-equivalence of the large deviations of the derived models and the microscopic process as defined by their action functionals. Hence, apart from the local error, we are interested in the long time behavior of the derived approximation processes including rare events and phase transitions. It was shown in [21], where an action functional for the mean field Ising model was derived, that the asymptotic equivalence of the action functionals between two processes implies that the processes have similar

[2]See the remark at the end of this subsection for such an example.

dynamical properties and particularly they have the same probability of rare events and exit times.

In this Section, a time dependent action functional is derived for the DLM. Similar computations for the variants of DLM give the same asymptotic behavior thus they are omitted. We show that the action functional for DLM is asymptotically equivalent to the action functional derived in [33] and briefly revised at the end of the Section 2.4 where large deviations for a system of long range interactions that models diffusion of interacting particles was studied. The results in [33] where an extension of the large deviation results in [35] in which Kawasaki dynamics (i.e. diffusion) for short range interactions was examined. Since DLM is a space discretization of the SPDE (a.k.a. the action functional of the microscopic model) it is straightforward to show the asymptotic equivalence of the action functionals. Nevertheless, we present the detailed derivation for completeness.

In order to recover the action functional we have to identify a small parameter which will be sent to zero. In our case, the small parameter is the spacing of the discretization, $\frac{1}{m}$, or, in the context of coarse graining the size of a cell. Then for any absolutely continuous functions $\Psi : [0,1] \times [0,T] \to \mathbb{R}$ and $G : [0,1] \to \mathbb{R}$ the rate function is given by

$$S_{0T}^m(\Psi) = \int_0^T \Lambda^m(\Psi, \Psi_t) dt \tag{3.33}$$

where

$$\Lambda^m(\Psi, \Psi_t) = \sup_G \left\{ < g, \partial_t \Psi - m^2 u(\psi) >_{l^2} - \frac{1}{2} < g, q m^2 v v^T(\psi) g >_{l^2} \right\} , \tag{3.34}$$

while $g = \{g_k = G(x_k)\} \in \mathbb{R}^m$, similarly $\psi(t) = \{\psi_k(t) = \Psi(t, x_k) \in \mathbb{R}^m$ and $< \cdot, \cdot >_{l^2}$ is the usual l^2 inner product.

Using the asymptotic approximations (3.10) and (3.11) (i.e. the drift and the diffusion of the SPDE) it is straightforward to show that as $m \to \infty$

$$\begin{aligned} < g, \Psi_t - m^2 u(\psi), g > =& < G, \Psi_t - \partial_x \left\{ L[\Psi] (\frac{\partial_x \Psi}{\Psi(1-\Psi)} - \beta \partial_x (J * \Psi)) \right\} >_{l^2} \\ \to& < G, \Psi_t - \partial_x \left\{ L[\Psi] (\frac{\partial_x \Psi}{\Psi(1-\Psi)} - \beta \partial_x (J * \Psi)) \right\} >_{L^2} \end{aligned} \tag{3.35}$$

and

$$< g, q m^2(\psi) g >_{l^2} \to < \partial_x G, L[\Psi] \partial_x G >_{L^2} \tag{3.36}$$

Thus as $m \to \infty$ the asymptotic limit for $\Lambda^m(\Psi, \Psi_t)$ is

$$\Lambda(\Psi, \Psi_t) = \sup_G \left\{ \int_0^1 G \partial_x \left\{ L[\Psi] (\frac{\partial_x \Psi}{\Psi(1-\Psi)} - \beta \partial_x (J * \Psi)) \right\} dx - \int_0^1 L[\Psi] (\partial_x G)^2 dx \right\} \tag{3.37}$$

Using Γ-convergence arguments and the arguments in [33], a rigorous proof of the above result could be carried out. In order to establish the equivalence between the action functional derived here and the action functional for the microscopic process derived in [33] we should think (3.37) as a maximization problem and use the calculus of variation theory. Thus denoting $H(x,t)$ the maximizer of (3.37), we have by

definition that for any appropriate test function Φ

$$\begin{aligned} 0 = \frac{d}{d\epsilon}\{ &< H + \epsilon\Phi, \partial_t\Psi - \partial_x\{L[\Psi](\frac{\partial_x\Psi}{\Psi(1-\Psi)} - \beta\partial_x(J*\Psi))\} >_{L^2} \\ &< \partial_x\{H+\epsilon\Phi\}L[\Psi], \partial_x\{H+\epsilon\Phi\} >_{L^2}\} \end{aligned} \tag{3.38}$$

which can be written as

$$\begin{aligned} \partial_t\Psi &= \partial_x\left\{L[\Psi](\frac{\partial_x\Psi}{\Psi(1-\Psi)} - \beta\partial_x(J*\Psi))\right\} + 2\partial_x\{L[\Psi]\partial_x H\} \\ &= \partial_x\left\{L[\Psi](\frac{\partial_x\Psi}{\Psi(1-\Psi)} - \beta\partial_x(J*\Psi - \frac{2}{\beta}H))\right\} \end{aligned} \tag{3.39}$$

Substituting (3.39) into (3.37) follows that

$$\Lambda(\Psi, \Psi_t) =< \partial_x H, L[\Psi]\partial_x H >_{L^2} \tag{3.40}$$

and thus the rate function equals in the limit to

$$S_{0T}(\Psi) = \int_0^T \int_0^1 L[\Psi](\partial_x H)^2 dxdt \tag{3.41}$$

which is exactly the microscopic action functional given by (2.33).

Remark: While for exchange (i.e. Kawasaki) dynamics the action functionals between the Langevin approximations and the underlying microscopic process are asymptotically equivalent, this is not true for adsorption/desorption (i.e. Glauber) dynamics. Indeed, both Langevin approximation [30], [20] and Hanggi correction [34] result in action functional which are asymptotically different from the action functional of the underlying microscopic process derived in [21, p. 146]. Moreover, the action functionals of an SDE driven process is generally of weighted quadratic form [32] while the action functional of the microscopic adsorption/desorption process is far more complex. However, using as a starting point for Langevin approximation the discretization of the microscopic action functional –similar to what we did in this paper– there might be a way to construct accurate Langevin approximations whose action functionals are asymptotically equivalent to the microscopic adsorption/desorption process.

4. Numerical Results. The objective of this Section is to study pattern formation in surface diffusion using the proposed Langevin-type models. Since the stochastic fluctuations of the proposed models are directly derived from the microscopic process, the exploration of the pattern morphologies on the complex energy landscape of the particle system is well emerged. Moreover, authors consider that it is important to promote reproducible research hence the code written for the production of the figures as well extended benchmark simulations is available online and it can be found at
`www.math.umass.edu/~pantazis/source/patternFormation_FigsCode.zip`

4.1. Numerical Schemes. In the previous Section space discretization (i.e. semi-discretization) was considered in detail. The final step in order to simulate the derived models on computers is to discretize the time, too. Since our primal goal is to highlight the space discretization, we keep the time discretization as simple as possible. Thus, a simple predictor-corrector (PC) Euler scheme which has 1st order weak convergence [23] is suggested. Of course implicit schemes or higher order

schemes such as Milstein's or derivative-free Runge-Kutta method could be used, however, they are computationally expensive especially for high dimensional systems such as the studied.

In order to highlight the implementation details, we restrict without loss of generality only to DLM. Then the PC Euler scheme at n-th iteration is given in matrix form by

$$\begin{aligned} \bar{X}_n &= X_n + u(\bar{X}_{n+1})\Delta t + v(X_n)\Delta W_n \\ X_{n+1} &= X_n + [(1-\alpha)u(X_n) + \alpha u(\bar{X}_n)]\Delta t + v(X_n)\Delta W_n \end{aligned} \tag{4.1}$$

where Δt is the time-step while ΔW_n is a vector of independent zero-mean Gaussians with covariance matrix $\Delta t I$. Initial value of the lattice configuration denoted by X_0 is also given while α is a weight factor which we set to 0.5 (trapezoidal rule). Since the size of the matrix v is $m^d \times m^d$ even though only $d+1$ of its diagonals are nonzero, it cannot be represented as a matrix in a computer memory hence we rewrite it – as well the drift term– in a compact implementable representation. For the general d-dimensional case, assume that $k = (k_1, ..., k_d)$ is a multi-index that denotes the position of the k-th variable an e_i is the unitary vector with 1 at position i. Then, the k-th element of the drift term is given by

$$\begin{aligned} u_k(X_n) = \sum_{i=1}^{d} \Bigg[& \frac{1}{2}(L_{k+e_i}(X_n) + L_k(X_n))(F_{k+e_i}(X_n) - F_k(X_n)) \\ & + \frac{1}{2}(L_k(X_n) + L_{k-e_i}(X_n))(F_k(X_n) - F_{k-e_i}(X_n)) \Bigg] \end{aligned} \tag{4.2}$$

where $F_k(X) = -\beta \bar{U}(k, X) + \log \frac{X(k)}{1-X(k)}$ while the k-th element of the stochastic term is given by

$$\begin{aligned} \sum_{l \in \mathcal{L}_m} v_{k,l}(X_n)\Delta W_n(l) = \sum_{i=1}^{d} \Bigg[& \sqrt{\frac{1}{q^d}(L_{k+e_i}(X_n) + L_k(X_n))}\Delta W_n^i(k) \\ & - \sqrt{\frac{1}{q^d}(L_k(X_n) + L_{k-e_i}(X_n))}\Delta W_n^i(k-e_i) \Bigg] \end{aligned} \tag{4.3}$$

where $W_n^i \sim N(0, \Delta t I_{m^d})$ is a zero-mean Gaussian vector while W_n^i and $W_{n'}^{i'}$ are independent random vectors.

In time discretization, similarly to space discretization, there are issues to be resolved. One such crucial issue is the choice of time step, Δt, which here were chosen heuristically using the following rule

$$\frac{1}{m^d} \sum_{k \in \mathcal{L}_m} |X_{n+1} - X_n| \approx \delta \tag{4.4}$$

which means that the average difference of the process in one step is controlled by δ. After many experiments on a large parameter regime, we set $\delta = 10^{-3}$ which is a compromise between stability and efficiency of the algorithm. Another artifact of time discretization is that the probability of X_{n+1} leaving the admissible domain $[0,1]^{m^d}$ is 1 making the algorithm to diverge. A simple solution to this problem is that whenever there is a element of X_{n+1} outside $[0,1]$ then the stochastic term is eliminated and only the drift term is considered. This is enough since the drift term

"push back" the value in the admissible interval. However, the cost to be paid is that we introduce bias which is proportional to the times the process leaves the admissible domain which of course depends on the time step, Δt. In our simulations, due to the specific choice of time step, the percentage of hitting the boundary values was less than 0.01%.

4.1.1. Sources of CPU Acceleration. The most time-consuming part of the numerical algorithm is the computation of the potential $\bar{U}(k, X_n)$ at each step for all $k \in \mathcal{L}_m$. This function is actually the convolution between the CG interaction potential and the lattice configuration. Thus an efficient method for computing the convolution between two function is through Fourier transform. Indeed, it holds that

$$\bar{U}(X_n) = \bar{J} * X_n = \mathcal{F}^{-1}\{\hat{\bar{J}}(\xi)\hat{X}_n(\xi)\} \tag{4.5}$$

where $\mathcal{F}^{-1}$ denotes the inverse Fourier transform while $\hat{\bar{J}}(\xi)$ and $\hat{X}_n(\xi)$ are the Fourier transforms of $\bar{J}$ and X_n, respectively.

Using multiplication in Fourier space instead of convolution in physical space makes the proposed method eventually independent of the interaction length. Indeed, the computational cost of one step of the numerical SDE solver is dropped from $O(M^d(L/q)^d)$ to $O(M^d \log M^d)$. Thus a huge computational gain is achieved for long range or mid range interaction potentials. This computational gain is a tremendous difference between the SDE approximations and the null event CGMC method which stems from the fact that in an SDE step the potential of all cells is needed while in a CGMC step the potential of only one cell is incorporated. Finally, the computation of convolution in Fourier space relates the proposed finite-difference method to the (pseudo-)spectral methods at least as concerns the computational cost.

4.2. Linear Stability Analysis. One fast and standard approach to roughly explore the behavior of the diffusive particle system at different parameter regimes is linear stability analysis of the mesoscopic PDE [36]. In connection with Fig. 2.1(a), linearized techniques belong to the mean-field class of models where most of the atomistic details have been integrated out. Generally, linear stability analysis identifies when a spatial perturbation added to a uniform solution of the PDE would either eliminate of grow in time [37], [38]. Thus if we disturb a constant solution of the mesoscopic PDE

$$\partial_t \rho = \nabla \cdot \left\{ L[\rho] \nabla \frac{\delta E}{\delta \rho} \right\} \tag{4.6}$$

by a spatially periodic perturbation of the form $e^{\lambda t} e^{i\xi x}$ then the dispersion relation between the perturbation growth rate, λ, and wavelength or mode, ξ, is given by

$$\lambda_\xi = T_0 ||\xi||^2 L[c_0] \left[\beta \hat{J}(\xi) - \frac{1}{c_0(1-c_0)} \right] \tag{4.7}$$

where $\hat{J}(\cdot)$ is the 2D Fourier transform of the continuous-space interaction potential, c_0 is the mean coverage and $L[c_0]$ is the mobility either of Metropolis or Arrhenius dynamics for the constant density function $\rho(t, x) = c_0$.

In order to observe phase transition phenomena –in our case pattern formation– there should exist positive growth rates. From (4.7) we could predict that phase transitions occur when there exists at least one wavenumber ξ' such that $\beta \hat{J}(\xi') \geq$

$\frac{1}{c_0(1-c_0)}$. Moreover, we could also predict from the same relation the most prominent size of the patterns. Indeed, the wavelength with the largest growth rate which is the wavelength that maximize the Fourier transform of the interaction potential (i.e., $\xi_{\max} = \text{argmax}_\xi \hat{J}(\xi)$) should dominate. Even though the following Section takes into account the information gained from linear stability analysis, it also reveals its limitations especially at critical parameter regimes.

4.3. Pattern Formation Simulations. In order to perform reliable benchmark simulations, it is necessary to utilize medium to large lattice domains. However, CGMC algorithm is prohibitively slow for large lattices resulting in the inability of providing sufficient statistics for comparison. Thus we perform limited benchmark simulations and relied on the theoretical results obtained in previous Sections. Nevertheless, we present the CPU time comparisons between CGMC algorithm and Langevin approximations. Table 4.1 shows the CPU execution time for null event CGMC algorithm and PLM2 model for Arrhenius dynamics. We prefer PLM2 model because it is the model with the most CPU-demanding (see (3.31)) among the Langevin models. It is evident from the Table that PLM2 scales linearly as the size of the lattice is increased while CGMC scales super-linearly due to the fact that the time step in CGMC is inverse proportional to the lattice size. Moreover, PLM2 is about 10-20 times faster from CGMC algorithm for relatively large lattices ($N = 2^9$) achieving a significant time acceleration.

	CGMC	PLM2
$N = 2^6$, $q = 2^2$	1.5×10^2	3.3×10^1
$N = 2^9$, $q = 2^2$	3.6×10^4	2.5×10^3

Table 4.1: CPU execution time in seconds of null event CGMC and PLM2 model for Arrhenius dynamics. Both algorithms run until final time $T = 100$. For $N = 2^6$ both algorithms have converge to equilibrium while they have not for $N = 2^9$.

Proceeding now to the study of pattern formation phenomena in surface diffusion, an appropriate interaction potential should be chosen. Following [39] and [36], patterns are formed when interaction potential is attractive at short range resulting in microphase separation and repulsive at long range so as they do not coalescence. A typical choice of attractive/repulsive interaction potential is Morse potential given in a general form by

$$J_1(x-y;\chi_1,r_{a,1},r_{r,1},J_1) := \frac{J_1}{2\pi r_{a,1}^2}\exp\left(-\frac{||x-y||}{r_{a,1}}\right) - \frac{J_1\chi_1}{2\pi r_{r,1}^2}\exp\left(-\frac{||x-y||}{r_{r,1}}\right) \tag{4.8}$$

where J_1 is the potential strength while $r_{a,1}$ and $r_{r,1}$ are the attractive and repulsive length scales. Note that in order to have short range attractive and long range repulsive interaction potential it should hold $r_{r,1} > r_{a,1}$. The ratio between attractive and repulsive forces is determined by the repulsion strength, χ_1. The 2D Fourier transform of Morse potential is

$$\hat{J}_1(\xi) = J_1\frac{1}{1+r_{a,1}^2||\xi||^2} - J_1\chi_1\frac{1}{1+r_{r,1}^2||\xi||^2} \tag{4.9}$$

hence based on linear stability analysis the most prominent wavelength is the maxi-

mum of the Fourier transform of the interaction potential given by

$$||\xi_1^{\max}|| = \frac{1}{r_{a,1}}\sqrt{\frac{\sqrt{\chi_1 R_1}-1}{R_1-\sqrt{\chi_1 R_1}}} \tag{4.10}$$

where $R_1 = \frac{r_{r,1}^2}{r_{a,1}^2} > 1$ and it should hold $1 < \sqrt{\chi_1 R_1} < R_1$ so as a real-valued dominant mode is obtained. Moreover, the rate of growth of the dominant pattern size which is crucially determined from the value of the interaction potential at mode $\xi_1^{\max}$ (see (4.7)) equals

$$\hat{J}_1(\xi_1^{\max}) = J_1 \frac{R_1-\sqrt{\chi_1 R_1}}{R_1-1}\left(1-\frac{\chi_1}{1-\sqrt{\chi_1 R_1}}\right) \tag{4.11}$$

However, the decay of the Fourier transform of the interaction potential is of polynomial order which is slow and under the presence of stochastic fluctuations patterns are irregular. In order to obtain nearly periodic configurations another interaction potential which is also called Morse potential should be utilized. In recent years, this potential had been applied for the study of pattern formation [40], [12] and it is defined as the difference of two Gaussian kernels, i.e.

$$J_2(x-y;\chi_2,r_{a,2},r_{r,2},J_2) := \frac{J_2}{2\pi r_{a,2}^2}\exp\left(-\frac{||x-y||^2}{2r_{a,2}^2}\right) - \frac{J_2\chi_2}{2\pi r_{r,2}^2}\exp\left(-\frac{||x-y||^2}{2r_{r,2}^2}\right) \tag{4.12}$$

where, similar to previous interaction potential, J_2 is the potential strength, χ_2 is the repulsion strength while $r_{a,2}$ and $r_{r,2}$ are dimensionless length scales or attraction and repulsion, respectively. The 2D Fourier transform of this variant of the Morse potential is given by

$$\hat{J}_2(\xi) = J_2\exp\left(-\frac{r_{a,2}^2||\xi||^2}{2}\right) - J_2\chi_2\exp\left(-\frac{r_{r,2}^2||\xi||^2}{2}\right) \tag{4.13}$$

which is again a difference of two Gaussian kernels. Notice that the decay rate of the Fourier modes are now exponential. Since our primal interest is to produce configurations of patterns which are stable and nearly periodic we present most of our results using $J_2(\cdot)$. Moreover, the most prominent size of the patterns is related to the maximum value of the Fourier transform of $J_2(\cdot)$ and it is obtained at

$$||\xi_2^{\max}|| = \frac{1}{r_{a,2}}\sqrt{\frac{2\ln\chi_2 R_2}{(R_2-1)}} \tag{4.14}$$

where $R_2 = \frac{r_{r,2}^2}{r_{a,2}^2} > 1$ is the repulsive to attractive ratio while it should hold $\chi_2 R_2 > 1$. The growth rate of the dominant wavelength is given by

$$\hat{J}_2(\xi_2^{\max}) = J_2(\chi R_2)^{\frac{1}{1-R_2}}(1-R_2^{-1}) \tag{4.15}$$

The study of pattern formation is performed using the variant of Morse potential, $J_2(\cdot)$. Fig. 4.1 shows configurations of the system at equilibrium for various parameter values. Specifically, the size of the lattice is $N = 2^9$ while the coarsening factor is $q = 4$. Interaction strength is $J_2 = 1$ with inverse temperature is $\beta = 12$. Attraction

and repulsion length-scales are set to $r_{a,2} = 5$ and $r_{r,2} = 10$, respectively, while two different repulsion strengths, $\chi_2 = 0.4$ (left column) and $\chi_2 = 0.8$ (right column) are applied. Arrhenius dynamics with diffusion rate $d_\beta = 0.27$ is used for this simulation while the preferred numerical scheme was PLM2 with step size suitably chosen for each case such that (4.4) is approximately valid.

Based on linear stability analysis, we expect that patterns do occur for Fig 4.1(a),(c), (d)&(e) but not for Fig 4.1(b)&(f) because the growth rate as it is calculated from the dispersion relation (4.7) is negative for all modes. However as it is evident from the figure, patterns are formed in any case. Of course, patterns in Fig 4.1(b)&(f) are much more noisy exactly due to the fact that the growth rate of the dominant wavelength is (positive but) very small. Furthermore, the stochastic fluctuations of the model are important since patterns with different sizes are observed in each configuration. This result is in accordance with the CGMC runs performed in [36] and it is far from the configurations obtained when deterministic models [12] were used where patterns are almost uniform. Additionally, changing the mean coverage, c_0, dots, labyrinths and inverted dots are observed. Similar experimental images were shown in [27] where surface diffusion of lead (Pt) on a copper (Cu) layer were studied. A final observation is that looking at the two columns of the Figure, the size of the patterns is decreased as repulsion strength, χ_2, is increased as it is expected from (4.14) since the dominant size of the patterns is inverse proportional to the wavelength. Intuitively, it can be also explained by the fact that strong long range repulsion leads to even less coalescence of patterns as time evolves.

The final numerical experiment of this section is the comparison of the two attractive/repulsive interaction potentials $J_1(\cdot)$ and $J_2(\cdot)$. The motivation for this experiment stems from the fact that even though the prominent size of the patterns are chosen to be equal –based on linear stability analysis– for both potentials, the behavior of the overall system is expected to be different due to the different decay of the modes. As already stated, the decay of the modes for $J_1(\cdot)$ is polynomial while the decay of the modes for $J_2(\cdot)$ is exponential hence we expect that the use of $J_1(\cdot)$ will produce a richer class of patterns making for instance the control of the size a rather difficult task. The configurations obtained at equilibrium using the Morse potential $J_1(\cdot)$ as well its variant $J_2(\cdot)$ are shown in Fig. 4.2(a) and (b), respectively. The control parameters of the interaction potentials was appropriately chosen so as the dominant modes of the Fourier transform be equal (i.e. $\xi_1^{\max} = \xi_2^{\max} = 0.15$) as well their growth rates be equal (i.e. $\hat{J}_1(\xi_1^{\max}) = \hat{J}_2(\xi_2^{\max}) = 1$). In order to specify all the parameters of the interaction potentials we further set $\chi_1 = \chi_2 = 0.5$ and $R_1 = R_2 = 4$ while the remaining parameters of the system are set to $\beta = 10$ and $d_\beta = 0.5$.

By visual inspection of Fig. 4.2, it can be stated that the distribution of the sizes of the patterns is more diverse for the original Morse potential compared to its variant. Moreover, as the histograms of the radius of the patterns suggest, the prominent radius in both potentials is 6 lattice sites which is comparable to the expected radius of the patterns being in this case $\frac{1}{\xi^{\max}} = \frac{1}{0.15} = 6.6$ lattice sites. Finally, one simple approach to quantify the diversity of the pattern sizes is to compute the standard deviation of the radius of the patterns which is 2.4 and 2.0 for the original Morse potential and its variant, respectively. Overall, as it was predicted by linear stability analysis, original Morse potential produce a larger class of pattern sizes compared to its variant.

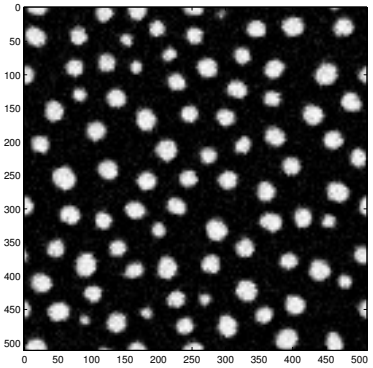

(a) $c_0 = 0.2$ & $\chi_2 = 0.4$

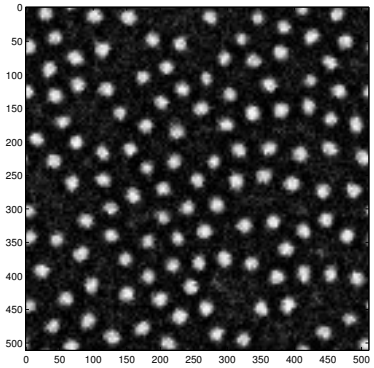

(b) $c_0 = 0.2$ & $\chi_2 = 0.8$

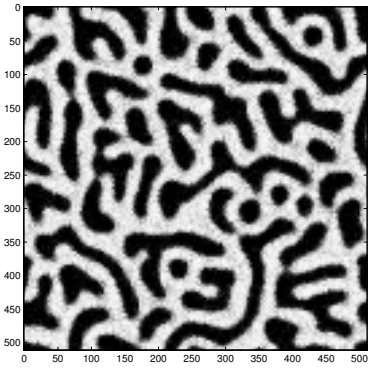

(c) $c_0 = 0.5$ & $\chi_2 = 0.4$

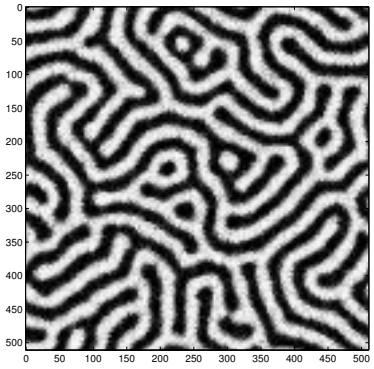

(d) $c_0 = 0.5$ & $\chi_2 = 0.8$

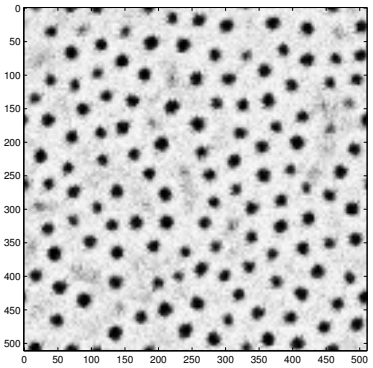

(e) $c_0 = 0.8$ & $\chi_2 = 0.4$

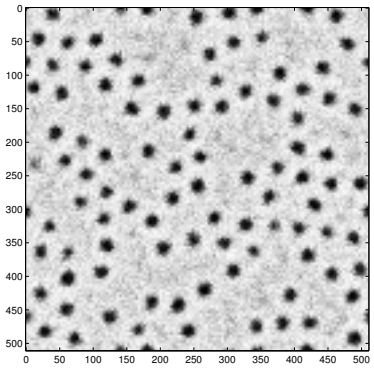

(f) $c_0 = 0.8$ & $\chi_2 = 0.8$

Fig. 4.1: A huge variety of patterns (dots, labyrinths, inverted dots) are produced at different parameter regimes corresponding to the complex landscape created by the competing interactions and the various conserved surface coverages, c_0. Also, quantities such as the size of the patterns can be controlled by the system's parameters.

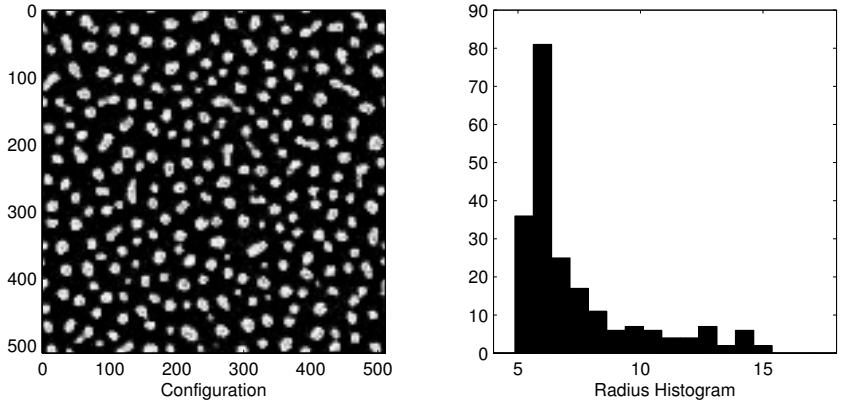

(a) Applying J_1 of (4.8)

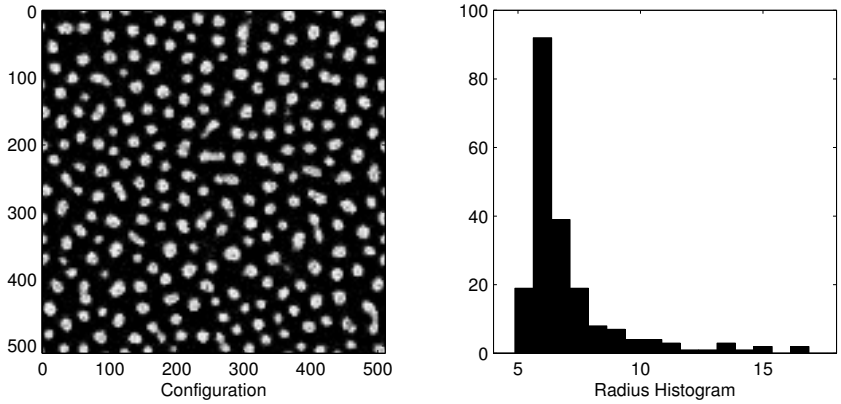

(b) Applying J_2 of (4.12)

Fig. 4.2: Using different attractive/repulsive interaction potentials configurations with different characteristics are obtained.

5. Conclusions. In this paper, we derived models which served as approximations of the CG process for the study of pattern formation on surfaces. Our starting point was an appropriate space discretization of the SPDE which lead to a system of SDE of Langevin type. Inspired by both the microscopic level and the mesoscopic level, the proposed models inherit properties from both levels. Indeed, (a) finite time estimates on the weak error between CG process and the process driven by the proposed models were obtained, (b) we showed that the action functionals between the microscopic model and the proposed are asymptotically equivalent which is a direct consequence of the fact that the proposed models are a direct discretization of the action functional (i.e. of the SPDE) and (c) by a perturbation of order $O(\frac{1}{q^d})$ either to the drift or the invariant measure, the derived models satisfied DBC hence the invariant measure of the approximation process is known. Hence the derived approximation models control the error at finite, long and infinite time scales.

Additionally, the knowledge of the invariant measure revealed a very interesting observation –to our best knowledge never stated before– which says that the space

discretization of the SPDE for Metropolis dynamics lead to a system whose temperature was perturbed by a factor of $\frac{1}{q}$. This observation asserts that the discretization of a SPDE may produce artifacts and bias to the numerical results when q is small. Moreover, increasing or decreasing the power of the noise, which is straightforward for the suggested models by suitably scaling of the order parameters q and m, we are able to zoom in or out to more or less atomistic details of the system. In connection with Fig. 2.1(a), increasing or decreasing the power of the noise results in the translation of the models to the left towards microscopic level or to the right towards mesoscopic level, respectively. The controlled-error approximation and the microscopically derived fluctuations allow us to view the proposed models as "bridges" between molecular and continuum (S)PDE models of diffusion processes. Based on this reliable intermediate models, it may be possible to consider hybrid micro/macro models bridging the gap between algorithms with different spatial scales. We also refer to recent work in related hybrid models in fluctuation hydrodynamics [41].

Finally, as concerns the study of pattern formation phenomena through a self-assembly mechanism, we efficiently reproduce the sizes and types of patterns experimentally observed in previous studies [27]. The role of noise is critical for the systematic exploration of the complex energy landscape of the system. As it was evident from the Figures, the choice of the interaction potential as well the variation of the system's parameters significantly affects the size and the shape of the patterns. Additionally, having the invariant measure of the process, one of our next goals is to perform sensitivity analysis using the method developed by Majda and Gershgorin [22] which exploits the Fisher information at equilibrium. Furthermore, another important application we are interested in is the control of the pattern's properties. By varying the parameters of the system such as the mean concentration or the temperature or the repulsion strength in a controlled way we will be able to design patterns with specified shapes, sizes or even orientations. However, in order to perform optimal control we need appropriate mesoscopic observables for the patterns which is also under our research investigation. Particularly, defining appropriate mesoscopic observables using tools from image processing (see right column of Fig. 4.2 as a preliminary example of such tools) and pattern recognition is one of our immediate goals.

Acknowledgements. This work was supported, in part, by the National Science Foundation (USA, DMS-0715125, CMMI-0835673) and the EU project FP7-REGPOT-2009-1 "Archimedes Center for Modeling, Analysis and Computation". We would like to thank also Petr Plecháč, Luc Rey-Bellet and Dion Vlachos for the many, interesting and fruitful discussions.

REFERENCES

[1] D. P. Landau and K. Binder. *A guide to Monte Carlo simulations in statistical physics*. Cambridge University Press, 2000.

[2] H. Spohn. *Large scale dynamics of interacting particles*. Texts and Monographs in Physics. Springer-Verlag, Heidelberg, 1991.

[3] T.M. Liggett. *Interacting particle systems*. Springer - Berlin, 1985.

[4] M. A. Katsoulakis, A. J. Majda, and D. G. Vlachos. Coarse-grained stochastic processes and Monte Carlo simulations in lattice systems. *Journal of Computational Physics*, 186:250–278, 2003.

[5] M.A. Katsoulakis, A. Majda, and D. Vlachos. Coarse-grained stochastic processes for microscopic lattice systems. *Proc. Natl. Acad. Sci*, 100(3):782–782, 2003.

[6] M. A. Katsoulakis and D. G. Vlachos. Coarse-grained stochastic processes and kinetic Monte

Carlo simulators for the diffusion of interacting patricles. *Journal of Chemical Physics*, 119(18):9412–9427, 2003.

[7] M. A. Katsoulakis, P. Plecháč, and A. Sopasakis. Error analysis of coarse-graining for stochastic lattice dynamics. *SIAM J. Numerical Analysis*, 44(6):2270–2296, 2006.

[8] M. A. Katsoulakis, L. Rey-Bellet, P. Plecháč, and D. K. Tsagkarogiannis. Coarse-graining schemes and a posteriori error estimates for stochastic lattice systems. *ESAIM-Math. Model. Num. Analysis*, 41(3):627–660, 2007.

[9] E. Kalligiannaki, M.A. Katsoulakis, and P. Plecháč. Coupled coarse graining and Markov Chain Monte Carlo for lattice systems. 2010.

[10] A. DeMasi, E. Orlandi, E. Presutti, and L. Triolo. Glauber evolution with the Kac potentials. I. Mesoscopic and macroscopic limits, interface dynamics. *Nonlinearity*, 7(3):633–696, 1994.

[11] G. Giacomin and J. L. Lebowitz. Exact microscopic description of phase segregation in model alloys with long-range interaction. *Physics Review Letter*, 76:1094–1097, 1996.

[12] N.M. Abukhdeir, D.G. Vlachos, M.A. Katsoulakis, and M. Plexousakis. Long-time integration methods for mesoscopic models of pattern-forming systems. *J. Comp. Phys.*, 230:5704–5715, Jun 2011.

[13] M. Hildebrand and A.S. Mikhailov. Mesoscopic modeling in the kinetic theory of adsorbates. *J. Chem. Phys.*, 100:19089, 1996.

[14] I. Gyöngy. Lattice approximations for stochastic quasi-linear parabolic partial differential equations driven by space-time white noise II. *Potential Analysis*, 11:1–37, 1999.

[15] D.G. Vlachos and M.A. Katsoulakis. Derivation and validation of mesoscopic theories for diffusion of interacting molecules. *Phys. Rev. Letters*, 85(18):3898–3901, 2000.

[16] M. Hildebrand. Self-organized nanostructures in surface chemical reactions: Mechanisms and mesoscopic modeling. *Chaos*, 12:144–156, 2002.

[17] D.J. Horntrop. Mesoscopic simulation of Ostwald ripening. *J. Comp. Phys.*, 218:429–441, 2006.

[18] D. T. Gillespie. The chemical Langevin equation. *J. Chem. Phys.*, 113:297–306, 2000.

[19] A. L.-S. Chua, C. A. Haselwandter, C. Baggio, and D. D. Vvedensky. Langevin equations for fluctuating surfaces. *Phys. Rev. E*, 72:051103 1–15, 2005.

[20] S. Are, M.A. Katsoulakis, and A. Szepessy. Coarse-grained Langevin approximations and spatiotemporal acceleration for kinetic Monte Carlo simulations of diffusion of interacting particles. *Chinese annals of mathematics. Series B*, 30:653–682, 2009.

[21] F. Comets. Nucleation for a long range magnetic model. *Probabilités et Statistiques*, 23(2):135–178, 1987.

[22] A. J. Majda and B. Gershgorin. Quantifying uncertainty in climate change science through empirical information theory. In *Proc. of the National Academy of Science*, 2010.

[23] P. E. Kloeden and E. Platen. *Numerical Solution of Stochastic Differential Equations*. Springer-Verlag, 1992.

[24] M.C. Cross and P.C. Hohenberg. Pattern formation outside of equilibrium. *Reviews of Modern Physics*, 65(3):851–1111, 1993.

[25] R. Hoyle. *Pattern Formation: An Introduction to Methods*. Cambridge University Press, 2006.

[26] R. Choksi, M. Maras, and J.F. Williams. 2D phase diagram for minimizers of a Cahn-Hilliard functional with long-range interactions. *SIAM J. Applied Dynamical Systems*, 2011.

[27] R. Plass, J. Last, N. Bartelt, and G. Kellogg. Self-assembled domain patterns. *Nature*, 412:1975, 2001.

[28] H. C. Kang and W. H. Weinberg. Dynamic Monte Carlo with a proper energy barrier: Surface diffusion and two-dimensional domain ordering. *J. Chem. Phys.*, 90:2824–2830, 1989.

[29] H. C. Kang and W. H. Weinberg. Modeling the kinetics of heterogeneous catalysis. *Chem. Rev.*, 95:667–676, 1995.

[30] M. A. Katsoulakis and A. Szepessy. Stochastic hydrodynamical limits of particle systems. *Commun. Math. Sci.*, 4(3):513–549, 2006.

[31] T. G. Kurtz. *Approximation of population processes*. Society for Industrial and Applied Mathematics (SIAM), 1981.

[32] M. I. Freidlin and A. D. Wentzell. *Random Perturbations of Dynamical Systems*. Springer-Verlag, 1998.

[33] A. Asselah and G. Giacomin. Metastability for the exclusion process with mean-field interaction. *J. Stat. Phys.*, 93:1051–1110, 1998.

[34] P. Hanggi, H. Grabert, P. Talkner, and H. Thomas. Bistable systems: Master equation versus Fokker-Planck modeling. *Phys. Rev. A*, 29:371–378, 1984.

[35] C. Kipnis, S. Olla, and S. R. S. Varadhan. Hydrodynamics and large deviation for simple exclusion processes. *Comm. on Pure and Applied Mathematics*, 42:115–137, 1989.

[36] A. Chatterjee and D. G. Vlachos. Systems tasks in nanotechnology via hierarchical multiscale modeling: Nanopattern formation in heteroepitaxy. *Chemical Engineering Science*,

62:4852–4863, 2007.
[37] P. Manneville. *Dissipative Structures and Weak Turbulence*. Academic Press, New York, 1990.
[38] G. Nicolis. *Introduction to nonlinear science*. Cambridge University Press, 1995.
[39] A. Stradner, H. Sedgwick, F. Cardinaux, W. C. K. Poon, S. U. Egelhaaf, and P. Schurtenberger. Equilibrium cluster formation in concentrated protein solutions and colloids. *Nature*, 432:492–495, 2004.
[40] A. Chatterjee and D. G. Vlachos. An overview of spatial microscopic and accelerated kinetic Monte Carlo methods for materials' simulation. *J. Computer-Aided Materials Design*, 14(2):253–308, 2007.
[41] A. Donev, J. B. Bell, A. L. Garcia, and B. J. Alder. A hybrid particle-continuum method for hydrodynamics of complex fluids. *Multiscale Modeling & Simulation*, 8:871–911, 2010.

Appendix A. Asymptotics. In order to compute the formal asymptotics of the drift term (3.2), diffusion matrix (3.5) and correction term (3.24) for both dynamics we need the following Taylor series expansions. Mobility is expanding up to the second order derivative given by

$$L_{k\pm1}(\rho) = L_k(\rho) \pm \frac{1}{m}\partial_x L_k(\rho) + \frac{1}{2m^2}\partial_{xx} L_k(\rho) + O(\frac{1}{m^3})$$

while potential is similarly expanded up to third order derivative by

$$\bar{U}(k\pm1,\rho) = \bar{U}(k,\rho) \pm \frac{1}{m}\partial_x \bar{U}(k,\rho) + \frac{1}{2m^2}\partial_{xx}\bar{U}(k,\rho) \pm \frac{1}{6m^3}\partial_{xxx}\bar{U}(k,\rho) + O(\frac{1}{m^4})$$

Finally, the difference of the logarithms which stems from the entropy term is expanded as

$$\begin{aligned}\log(\rho_{k\pm1}) - \log(\rho_k) = \pm\frac{1}{m}\frac{\partial_x\rho(x_k)}{\rho_k} + \frac{1}{2m^2}\left[\frac{\partial_{xx}\rho(x_k)}{\rho(x_k)} - \left(\frac{\partial_x\rho(x_k)}{\rho(x_k)}\right)^2\right] \\ \pm\frac{1}{6m^3}\left[\frac{\partial_{xxx}\rho(x_k)}{\rho(x_k)} - 3\frac{\partial_x\rho(x_k)\partial_{xx}\rho(x_k)}{\rho(x_k)^2} + 2\left(\frac{\partial_x\rho(x_k)}{\rho(x_k)}\right)^3\right] + O(\frac{1}{m^4})\end{aligned}$$

and similarly for $\log(1-\rho_k) - \log(1-\rho_{k\pm1})$.

Now, we are able to compute the formal asymptotic for the drift term as

$$\begin{aligned}
u_k(\rho) &= \frac{1}{2}(L_{k+1}(\rho)+L_k(\rho))\{-\beta[\bar{U}(k+1,\rho)-\bar{U}(k,\rho)] + [\log(\rho(x_{k+1})) - \log(\rho(x_k))] - [\log(1-\rho(x_{k+1})) - \log(1-\rho(x_k))]\} \\
&+ \frac{1}{2}(L_k(\rho)+L_{k-1}(\rho))\{-\beta[\bar{U}(k-1,\rho)-\bar{U}(k,\rho)] + [\log(\rho(x_{k-1})) - \log(\rho(x_k))] - [\log(1-\rho(x_{k-1})) - \log(1-\rho(x_k))]\} \\
&= \frac{1}{2}\left[2L_k(\rho) + \frac{1}{m}\partial_x L_k(\rho) + \frac{1}{2m^2}\partial_{xx}L_k(\rho)\right] \times \left\{\frac{-\beta}{m}\partial_x\bar{U}(k,\rho) + \frac{-\beta}{2m^2}\partial_{xx}\bar{U}(k,\rho) + \frac{-\beta}{6m^3}\partial_{xxx}\bar{U}(k,\rho)\right. \\
&+ \frac{1}{m}\frac{\partial_x\rho(x_k)}{\rho_k} + \frac{1}{2m^2}\left[\frac{\partial_{xx}\rho(x_k)}{\rho(x_k)} - \left(\frac{\partial_x\rho(x_k)}{\rho(x_k)}\right)^2\right] + \frac{1}{6m^3}\left[\frac{\partial_{xxx}\rho(x_k)}{\rho(x_k)} - 3\frac{\partial_x\rho(x_k)\partial_{xx}\rho(x_k)}{\rho(x_k)^2} + 2\left(\frac{\partial_x\rho(x_k)}{\rho(x_k)}\right)^3\right] \\
&+ \left.\frac{1}{m}\frac{\partial_x\rho(x_k)}{1-\rho_k} + \frac{1}{2m^2}\left[\frac{\partial_{xx}\rho(x_k)}{1-\rho(x_k)} + \left(\frac{\partial_x\rho(x_k)}{1-\rho(x_k)}\right)^2\right] + \frac{1}{6m^3}\left[\frac{\partial_{xxx}\rho(x_k)}{1-\rho(x_k)} + 3\frac{\partial_x\rho(x_k)\partial_{xx}\rho(x_k)}{(1-\rho(x_k))^2} + 2\left(\frac{\partial_x\rho(x_k)}{1-\rho(x_k)}\right)^3\right]\right\} \\
&+ \frac{1}{2}\left[2L_k(\rho) - \frac{1}{m}\partial_x L_k(\rho) + \frac{1}{2m^2}\partial_{xx}L_k(\rho)\right] \times \left\{\frac{-\beta}{m}\partial_x\bar{U}(k,\rho) + \frac{-\beta}{2m^2}\partial_{xx}\bar{U}(k,\rho) - \frac{-\beta}{6m^3}\partial_{xxx}\bar{U}(k,\rho)\right. \\
&- \frac{1}{m}\frac{\partial_x\rho(x_k)}{\rho_k} + \frac{1}{2m^2}\left[\frac{\partial_{xx}\rho(x_k)}{\rho(x_k)} - \left(\frac{\partial_x\rho(x_k)}{\rho(x_k)}\right)^2\right] - \frac{1}{6m^3}\left[\frac{\partial_{xxx}\rho(x_k)}{\rho(x_k)} - 3\frac{\partial_x\rho(x_k)\partial_{xx}\rho(x_k)}{\rho(x_k)^2} + 2\left(\frac{\partial_x\rho(x_k)}{\rho(x_k)}\right)^3\right] \\
&- \left.\frac{1}{m}\frac{\partial_x\rho(x_k)}{1-\rho_k} + \frac{1}{2m^2}\left[\frac{\partial_{xx}\rho(x_k)}{1-\rho(x_k)} + \left(\frac{\partial_x\rho(x_k)}{1-\rho(x_k)}\right)^2\right] - \frac{1}{6m^3}\left[\frac{\partial_{xxx}\rho(x_k)}{1-\rho(x_k)} + 3\frac{\partial_x\rho(x_k)\partial_{xx}\rho(x_k)}{(1-\rho(x_k))^2} + 2\left(\frac{\partial_x\rho(x_k)}{1-\rho(x_k)}\right)^3\right]\right\} + O(\frac{1}{m^4}) \\
&= \frac{1}{m^2}L_k(\rho)\left[-\beta\partial_{xx}\bar{U}(k,\rho) + \frac{\partial_{xx}\rho(x_k)}{\rho(x_k)} - \left(\frac{\partial_x\rho(x_k)}{\rho(x_k)}\right)^2 + \frac{\partial_{xx}\rho(x_k)}{1-\rho(x_k)} + \left(\frac{\partial_x\rho(x_k)}{1-\rho(x_k)}\right)^2\right] \\
&+ \frac{1}{m^2}\partial_x L_k(\rho)\left[-\beta\partial_x\bar{U}(k,\rho) + \frac{\partial_x\rho(x_k)}{\rho_k} + \frac{\partial_x\rho(x_k)}{1-\rho_k}\right] + O(\frac{1}{m^4}) \\
&= \frac{1}{m^2}\partial_x\left\{L_k(\rho)\left[-\beta\partial_x\bar{U}(k,\rho) + \frac{\partial_x\rho(x_k)}{\rho(x_k)(1-\rho(x_k))}\right]\right\} + O(\frac{1}{m^4})
\end{aligned} \tag{A.1}$$

Similarly, the weak form of the diffusion matrix (i.e. covariance matrix) has the following formal asymptotic

$$
\begin{aligned}
&\left\langle \sum_{k,j} b^T_{j,k}\phi_1(x_j)\frac{dW_k}{dt}, \sum_{l,i} b^T_{i,l}\phi_2(x_i)\frac{dW_l}{dt} \right\rangle = \sum_{k,l} D_{k,l}\phi_1(x_k)\phi_2(x_l) \\
&= \sum_k \left[D_{k,k-1}\phi_2(x_{k-1}) + D_{k,k}\phi_2(x_k) + D_{k,k+1}\phi_2(x_{k+1})\right]\phi_1(x_k) \\
&= \sum_k \left[D_{k,k-1}(\phi_2(x_{k-1}) - \phi_2(x_k))(\phi_1(x_{k-1}) - \phi_1(x_k))\right] \\
&= \frac{1}{q}\sum_k \left[(L_{k-1} + L_k)(\phi_2(x_{k-1}) - \phi_2(x_k))(\phi_1(x_{k-1}) - \phi_1(x_k))\right] \\
&= \frac{1}{q}\sum_k L_k \left[(\phi_2(x_{k-1}) - \phi_2(x_k))(\phi_1(x_{k-1}) - \phi_1(x_k)) + (\phi_2(x_{k+1}) - \phi_2(x_k))(\phi_1(x_{k+1}) - \phi_1(x_k))\right] \\
&= \frac{1}{q}\sum_k L_k \left[\left(\frac{1}{m}\partial_x\phi_2(x_k) - \frac{1}{2m^2}\partial_{xx}\phi_2(x_k) + O(1/m^3)\right)\left(\frac{1}{m}\partial_x\phi_1(x_k) - \frac{1}{2m^2}\partial_{xx}\phi_1(x_k) + O(1/m^3)\right)\right. \\
&+ \left.\left(\frac{1}{m}\partial_x\phi_2(x_k) + \frac{1}{2m^2}\partial_{xx}\phi_2(x_k) + O(1/m^3)\right)\left(\frac{1}{m}\partial_x\phi_1(x_k) + \frac{1}{2m^2}\partial_{xx}\phi_1(x_k) + O(1/m^3)\right)\right] \\
&= \frac{1}{q}\sum_k 2L_k \left[\frac{1}{m^2}\partial_x\phi_1(x_k)\partial_x\phi_2(x_k) + O(1/m^4)\right] \\
&= \frac{2}{qm}\int L(\rho(x))\partial_x\phi_1(x)\partial_x\phi_2(x)dx + O(1/m^4)
\end{aligned}
\tag{A.2}
$$

Finally, the asymptotic expansion of the "correction" term for Arrhenius dynamics can be alternatively written as

$$
\begin{aligned}
C_k(\rho) &= \frac{1}{m^2}\partial_{xx}\left\{(1-2\rho(x_k))\exp(-\beta\bar{U}(k,\rho)) - \beta q(\bar{J}(0)+\bar{J}(1))L_k(\rho)\right\} + O(\frac{1}{m^4}) \\
&= \frac{1}{m^2}\partial_x\left\{-2\partial_x\rho(x_k)\exp(-\beta\bar{U}(k,\rho)) - \beta(1-2\rho(x_k))\partial_x\bar{U}(k,\rho)\exp(-\beta\bar{U}(k,\rho))\right. \\
&- \left.\beta q(\bar{J}(0)+\bar{J}(1))[(1-2\rho(x_k))\partial_x\rho(x_k)\exp(-\beta\bar{U}(k,\rho)) - \beta\partial_x\bar{U}(k,\rho)L_k(\rho)]\right\} + O(\frac{1}{m^4}) \\
&= \frac{1}{m^2}\partial_x\left\{\left(\frac{-2\partial_x\rho(x_k)}{\rho(x_k)(1-\rho(x_k))} + \beta^2 q(\bar{J}(0)+\bar{J}(1))\partial_x\bar{U}(k,\rho)\right.\right. \\
&- \left.\left.\beta\frac{1-2\rho(x_k)}{\rho(x_k)(1-\rho(x_k))}(q(\bar{J}(0)+\bar{J}(1))\partial_x\rho(x_k) + \partial_x\bar{U}(k,\rho))\right)L_k(\rho)\right\} + O(\frac{1}{m^4})
\end{aligned}
\tag{A.3}
$$

Appendix B. Detailed Balance Condition and Discrete Free Energy Decrease. The computation of the inner products shown in (3.16) is given next. After an integration by parts and taking advantage of the periodic boundary condition

879 we obtain that

$$
\begin{aligned}
&Z < \mathcal{M}f, g >_{L^2(\mu)} \\
&= \frac{1}{2q}\int \left[-\sum_{k\in\mathcal{L}_m} (L_{k+1}+L_k)\frac{\partial}{\partial\rho_{k+1}}\left(\frac{\partial f}{\partial\rho_k}e^{-q\bar{E}(\rho)}\right) g - \sum_{k\in\mathcal{L}_m}(L_k+L_{k-1})\frac{\partial}{\partial\rho_{k-1}}\left(\frac{\partial f}{\partial\rho_k}e^{-q\bar{E}(\rho)}\right) g \right. \\
&\left. + \sum_{k\in\mathcal{L}_m}(L_{k+1}+L_{k-1}+2L_k(\rho))\frac{\partial}{\partial\rho_k}\left(\frac{\partial f}{\partial\rho_k}e^{-q\bar{E}(\rho)}\right) g \right] \\
&= -\frac{1}{2q}\int \left[-\sum_{k\in\mathcal{L}_m} (L_{k+1}+L_k)\frac{\partial f}{\partial\rho_k}e^{-q\bar{E}(\rho)}\frac{\partial g}{\partial\rho_{k+1}} - \sum_{k\in\mathcal{L}_m}(L_k+L_{k-1})\frac{\partial f}{\partial\rho_k}e^{-q\bar{E}(\rho)}\frac{\partial g}{\partial\rho_{k-1}} \right. \\
&\left. + \sum_{k\in\mathcal{L}_m}(L_{k+1}+L_{k-1}+2L_k)\frac{\partial f}{\partial\rho_k}e^{-q\bar{E}(\rho)}\frac{\partial g}{\partial\rho_k} \right] - \frac{1}{2q}\int \sum_{k\in\mathcal{L}_m} C_k(\rho)\frac{\partial f}{\partial\rho_k} g e^{-q\bar{E}(\rho)} \\
&= -\frac{1}{2q}\int \left[-\sum_{k\in\mathcal{L}_m} (L_k+L_{k+1})\frac{\partial f}{\partial\rho_{k-1}}e^{-q\bar{E}(\rho)}\frac{\partial g}{\partial\rho_k} - \sum_{k\in\mathcal{L}_m}(L_{k+1}+L_k)\frac{\partial f}{\partial\rho_{k+1}}e^{-q\bar{E}(\rho)}\frac{\partial g}{\partial\rho_k} \right. \\
&\left. + \sum_{k\in\mathcal{L}_m}(L_{k+1}+L_{k-1}+2L_k)\frac{\partial f}{\partial\rho(x_k)}e^{-q\bar{E}(\rho)}\frac{\partial g}{\partial\rho(x_k)} \right] - \frac{1}{2q}\int \sum_{k\in\mathcal{L}_m} C_k(\rho)\frac{\partial f}{\partial\rho_k} g e^{-q\bar{E}(\rho)} \\
&= Z < f, \mathcal{M}g >_{L^2(\mu)} - \frac{1}{2q}\int \sum_{k\in\mathcal{L}_m} C_k(\rho)\left[\frac{\partial g}{\partial\rho_k}f + \frac{\partial f}{\partial\rho_k}g\right] e^{-q\bar{E}(\rho)}
\end{aligned}
\tag{B.1}
$$

880

881 Discrete free energy functional, $\bar{E}(\rho)$, is decreasing over time. Indeed, taking once
882 again advantage of the periodic boundary condition we obtain

$$
\begin{aligned}
&\frac{d}{dt}\bar{E}(\rho) = \sum_{k\in\mathcal{L}_m}\frac{\partial\bar{E}(\rho)}{\partial\rho_k}\frac{d\rho_k}{dt} \\
&= \frac{1}{2}\sum_{k\in\mathcal{L}_m}\frac{\partial\bar{E}(\rho)}{\partial\rho(x_k)}\left\{(L_{k+1}+L_k)\left[\frac{\partial\bar{E}(\rho)}{\partial\rho_{k+1}} - \frac{\partial\bar{E}(\rho)}{\partial\rho_k}\right] - (L_k+L_{k-1})\left[\frac{\partial\bar{E}(\rho)}{\partial\rho_k} - \frac{\partial\bar{E}(\rho)}{\partial\rho_{k-1}}\right]\right\} \\
&= \frac{1}{2}\sum_{k\in\mathcal{L}_m}(L_{k+1}+L_k)\frac{\partial\bar{E}(\rho)}{\partial\rho_k}\left[\frac{\partial\bar{E}(\rho)}{\partial\rho_{k+1}} - \frac{\partial\bar{E}(\rho)}{\partial\rho_k}\right] - \frac{1}{2}\sum_{k\in\mathcal{L}_m}(L_k+L_{k-1})\frac{\partial\bar{E}(\rho)}{\partial\rho_k}\left[\frac{\partial\bar{E}(\rho)}{\partial\rho_k} - \frac{\partial\bar{E}(\rho)}{\partial\rho_{k-1}}\right] \\
&= \frac{1}{2}\sum_{k\in\mathcal{L}_m}(L_{k+1}+L_k)\frac{\partial\bar{E}(\rho)}{\partial\rho_k}\left[\frac{\partial\bar{E}(\rho)}{\partial\rho_{k+1}} - \frac{\partial\bar{E}(\rho)}{\partial\rho_k}\right] - \frac{1}{2}\sum_{k\in\mathcal{L}_m}(L_{k+1}+L_k)\frac{\partial\bar{E}(\rho)}{\partial\rho_{k+1}}\left[\frac{\partial\bar{E}(\rho)}{\partial\rho_{k+1}} - \frac{\partial\bar{E}(\rho)}{\partial\rho_k}\right] \\
&= -\frac{1}{2}\sum_{k\in\mathcal{L}_m}(L_{k+1}+L_k)\left[\frac{\partial\bar{E}(\rho)}{\partial\rho_{k+1}} - \frac{\partial\bar{E}(\rho)}{\partial\rho_k}\right]^2 \leq 0
\end{aligned}
\tag{B.2}
$$

883 since mobility is always a non-negative function.